Report No. KS-15-09 ▪ FINAL REPORT▪ December 2015

Field Monitoring of Mechanically Stabilized Earth Walls to Investigate Secondary Reinforcement Effects

Yan Jiang
Jie Han, Ph.D., P.E.
Robert L. Parsons, Ph.D., P.E.
Hongyi Cai, Ph.D.

The University of Kansas

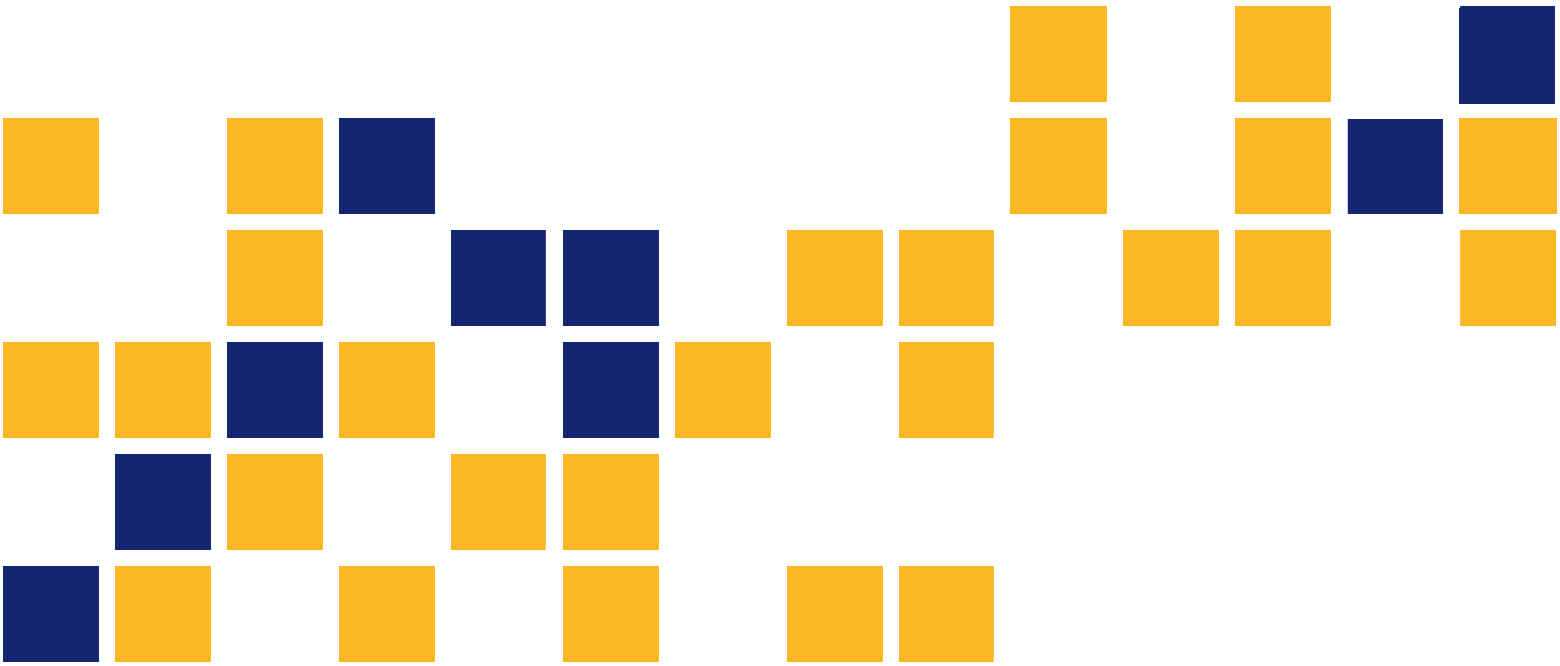

Kansas Department of Transportation

1 Report No. KS-15-09	**2 Government Accession No.**	**3 Recipient Catalog No.**
4 Title and Subtitle Field Monitoring of Mechanically Stabilized Earth Walls to Investigate Secondary Reinforcement Effects		**5 Report Date** December 2015 **6 Performing Organization Code**
7 Author(s) Yan Jiang, Jie Han, Ph.D., P.E., Robert L. Parsons, Ph.D., P.E., Hongyi Cai, Ph.D.		**7 Performing Organization Report No.**
9 Performing Organization Name and Address The University of Kansas Department of Civil, Environmental and Architectural Engineering 1530 West 15th St Lawrence, Kansas 66045-7609		**10 Work Unit No. (TRAIS)** **11 Contract or Grant No.** C1968
12 Sponsoring Agency Name and Address Kansas Department of Transportation Bureau of Research 2300 SW Van Buren Topeka, Kansas 66611-1195		**13 Type of Report and Period Covered** Final Report July 2013–July 2015 **14 Sponsoring Agency Code** RE-0642-01

15 Supplementary Notes
For more information write to address in block 9.
Appendices are available upon request to library@ksdot.org.

Mechanically stabilized earth (MSE) walls have been commonly used in highway construction. AASHTO (2007) has detailed design procedures for such a wall system. In the current AASHTO design, only primary reinforcements are used in relatively large spacing (commonly 2 feet), which requires higher connection strength between reinforcements and wall facing. Large spacing between reinforcements may also increase the chances of wall facing bulging and construction-related problems. To alleviate such problems, the use of secondary reinforcements installed between primary reinforcements was proposed. The use of secondary reinforcements could (1) reduce the required connection load for primary reinforcement, (2) increase the internal stability by secondary reinforcement, (3) improve the compaction near the wall facing, and (4) mitigate the down-drag behind the wall facing. However, this idea was not verified in practice.

To improve the understanding of the performance of MSE walls with secondary reinforcement and verify its benefits in practice, three MSE wall sections reinforced with geogrids were constructed and monitored in the field: (1) an MSE wall section with uniaxial geogrids as primary and secondary reinforcements, (2) an MSE wall section with uniaxial geogrids as primary reinforcements and with biaxial geogrids as secondary reinforcements, and (3) an MSE wall section with uniaxial geogrids as primary reinforcements only (i.e., the control section). Earth pressure cells, inclinometer pipes and a probe, and foil-type strain gauges were used in these three test wall sections to measure the vertical and lateral earth pressures, lateral wall facing deflections, and strains of primary and secondary geogrids, respectively. The measured results (i.e., the wall facing deflections, the vertical and horizontal earth pressures, and the strains of geogrids) were compared with those calculated using AASHTO (2007).

Based on the analysis of the field test results, major conclusions can be drawn in the following: (1) the secondary reinforcements reduced the wall facing deflections as compared with those in the control section; (2) the measured vertical earth pressures were close to the computed trapezoid stresses and increased with the construction of the wall; (3) the distribution of the measured lateral earth pressures in the control section linearly increased with depth, while the distributions of the measured lateral earth pressures in the sections with secondary reinforcements were approximately uniform with depth; (4) the measured tensile strains at the connection in all sections were small; and (5) secondary reinforcements reduced the maximum tensile strains in the primary geogrids.

17 Key Words Mechanically Stabilized Earth Walls, Secondary Reinforcements, Geogrids, Reinforcement Spacing		**18 Distribution Statement** No restrictions. This document is available to the public through the National Technical Information Service www.ntis.gov.	
19 Security Classification (of this report) Unclassified	**20 Security Classification (of this page)** Unclassified	**21 No. of pages** 90	**22 Price**

Form DOT F 1700.7 (8-72)

This page intentionally left blank.

Field Monitoring of Mechanically Stabilized Earth Walls to Investigate Secondary Reinforcement Effects

Final Report

Prepared by

Yan Jiang
Jie Han, Ph.D., P.E.
Robert L. Parsons, Ph.D., P.E.
Hongyi Cai, Ph.D.

The University of Kansas

A Report on Research Sponsored by

THE KANSAS DEPARTMENT OF TRANSPORTATION
TOPEKA, KANSAS

and

THE UNIVERSITY OF KANSAS
LAWRENCE, KANSAS

December 2015

PREFACE

The Kansas Department of Transportation's (KDOT) Kansas Transportation Research and New-Developments (K-TRAN) Research Program funded this research project. It is an ongoing, cooperative and comprehensive research program addressing transportation needs of the state of Kansas utilizing academic and research resources from KDOT, Kansas State University and the University of Kansas. Transportation professionals in KDOT and the universities jointly develop the projects included in the research program.

NOTICE

The authors and the state of Kansas do not endorse products or manufacturers. Trade and manufacturers names appear herein solely because they are considered essential to the object of this report.

This information is available in alternative accessible formats. To obtain an alternative format, contact the Office of Public Affairs, Kansas Department of Transportation, 700 SW Harrison, 2nd Floor – West Wing, Topeka, Kansas 66603-3745 or phone (785) 296-3585 (Voice) (TDD).

DISCLAIMER

The contents of this report reflect the views of the authors who are responsible for the facts and accuracy of the data presented herein. The contents do not necessarily reflect the views or the policies of the state of Kansas. This report does not constitute a standard, specification or regulation.

Abstract

Mechanically stabilized earth (MSE) walls have been commonly used in highway construction. AASHTO (2007) has detailed design procedures for such a wall system. In the current AASHTO design, only primary reinforcements are used in relatively large spacing (commonly 2 feet), which requires higher connection strength between reinforcements and wall facing. Large spacing between reinforcements may also increase the chances of wall facing bulging and construction-related problems. To alleviate such problems, the use of secondary reinforcements installed between primary reinforcements was proposed. The use of secondary reinforcements could (1) reduce the required connection load for primary reinforcement, (2) increase the internal stability by secondary reinforcement, (3) improve the compaction near the wall facing, and (4) mitigate the down-drag behind the wall facing. However, this idea was not verified in practice.

To improve the understanding of the performance of MSE walls with secondary reinforcement and verify its benefits in practice, three MSE wall sections reinforced with geogrids were constructed and monitored in the field: (1) an MSE wall section with uniaxial geogrids as primary and secondary reinforcements, (2) an MSE wall section with uniaxial geogrids as primary reinforcements and with biaxial geogrids as secondary reinforcements, and (3) an MSE wall section with uniaxial geogrids as primary reinforcements only (i.e., the control section). Earth pressure cells, inclinometer pipes and a probe, and foil-type strain gauges were used in these three test wall sections to measure the vertical and lateral earth pressures, lateral wall facing deflections, and strains of primary and secondary geogrids, respectively. The measured results (i.e., the wall facing deflections, the vertical and horizontal earth pressures, and the strains of geogrids) were compared with those calculated using AASHTO (2007).

Based on the analysis of the field test results, major conclusions can be drawn in the following: (1) the secondary reinforcements reduced the wall facing deflections as compared with those in the control section; (2) the measured vertical earth pressures were close to the computed trapezoid stresses and increased with the construction of the wall; (3) the distribution of the measured lateral earth pressures in the control section linearly increased with depth, while

the distributions of the measured lateral earth pressures in the sections with secondary reinforcements were approximately uniform with depth; (4) the measured tensile strains at the connection in all sections were small; and (5) secondary reinforcements reduced the maximum tensile strains in the primary geogrids.

Acknowledgements

The authors would like to acknowledge the financial support and field assistance from the Kansas Department of Transportation through the Kansas Transportation Research and New-Developments Program (K-TRAN) program. Mr. James J. Brennan, the Chief Geotechnical Engineer of KDOT, was the monitor for this project. Clarkson Construction Company provided great assistance and cooperation during wall instrumentation and monitoring. Tensar International provided geogrids for instrumentation. Technicians, Matthew Maksimowicz, David Woody, and Eric Nicholson, graduate students, Xiaohui Sun, Deep Khatri, Jun Guo, Omar K. Ismael, Fei Wang, Jamal Ismail Kakrasul, Ghaith Abdulrasool, Saif Jawad, and Mahdi Al-Naddaf, undergraduate students, Zack Brady and Nick Andrus, and visiting scholars, Mustapha Rahmaninezhad, Hongguang Zhang, Dan Chang, Fulin Li, and Hongbo Zhang from the University of Kansas provided great assistance in wall instrumentation and monitoring. All the above support and help are greatly appreciated.

Table of Contents

List of Tables

List of Figures

Chapter 1: Introduction

1.1 Background

A mechanically stabilized earth (MSE) wall consists of compacted backfill soil, geosynthetic or steel reinforcements, and a wall facing. The French engineer Henri Vidal was credited for the development of the modern MSE wall technology in 1960s. In the last four decades, the applications of MSE wall have dramatically grown in the world. Presently, approximately 40,000 MSE walls have been built in the United States (Koerner & Koerner, 2011). MSE walls can include metal or geosynthetic reinforcements. The metal reinforcements are often referred to as inextensible reinforcements. As compared with metal reinforcements, geosynthetic reinforcements have lower tensile stiffness and strength; therefore, they are referred to as extensible reinforcements.

The first MSE wall reinforced with geosynthetics was constructed in France in 1971. This MSE wall used geotextile and had a wrapped-around facing. It was reported that the first utilization of geogrids in MSE walls was in England in 1978. Since the 1980s, geosynthetics have been extensively used in MSE walls. For the two common geosynthetics, geogrids are more frequently utilized in MSE walls than geotextiles. In addition, approximately three-fourths of constructed MSE walls have modular block facings (Koerner & Koerner, 2011).

During construction of an MSE wall, reinforcements are installed in layers between compacted backfill soils to provide tensile resistance for backfill soils. Frictional or mechanical connections are commonly employed to connect reinforcements with wall facing. The wall facing can be wrapped-around, concrete panels, or modular blocks. Modular blocks are more commonly used with geosynthetics. Figure 1.1 shows a cross section of an MSE wall.

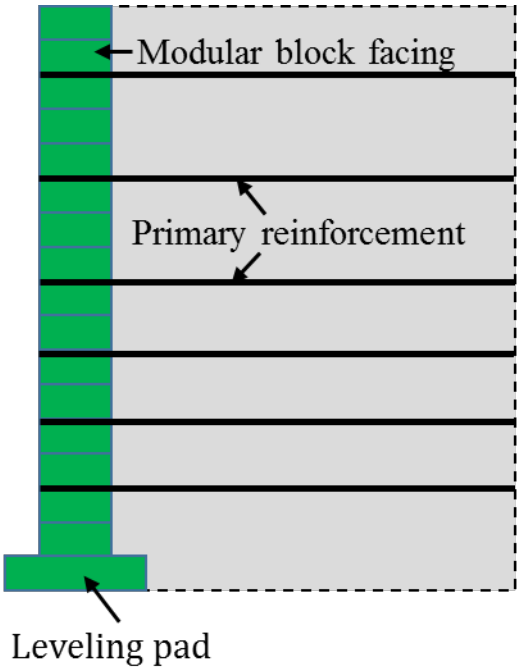

Figure 1.1: Cross Section of an MSE Wall

1.2 Problem Statements

Mechanically stabilized earth (MSE) walls have been commonly used in highway construction. AASHTO (2007) has detailed design procedures for such a wall system. In the current AASHTO design, only primary reinforcements are used in relatively large spacing (commonly 2 feet), which requires higher connection strength between reinforcements and wall facing. Large spacing between reinforcements may also increase the chances of wall facing bulging and construction-related problems. Leshchinsky (2000) suggested the use of short secondary reinforcements between primary reinforcements to alleviate connection load. Leshchinsky indicated that the use of secondary reinforcements may have the following benefits: (1) a reduction in required connection load for primary reinforcement, (2) an increase in the internal stability by the secondary reinforcement, (3) improved compaction near the wall facing, and (4) mitigation of down-drag behind the wall facing. As a result, the performance of MSE walls can be greatly enhanced. Vulova and Leshchinsky (2003) and Han and Leshchinsky (2006) conducted theoretical analyses to investigate the effects of secondary reinforcement on the behavior of MSE walls and confirmed the benefits of using secondary reinforcement to alleviate

connection loads and improve performance. So far, however, no field test has been performed to verify the theoretical results.

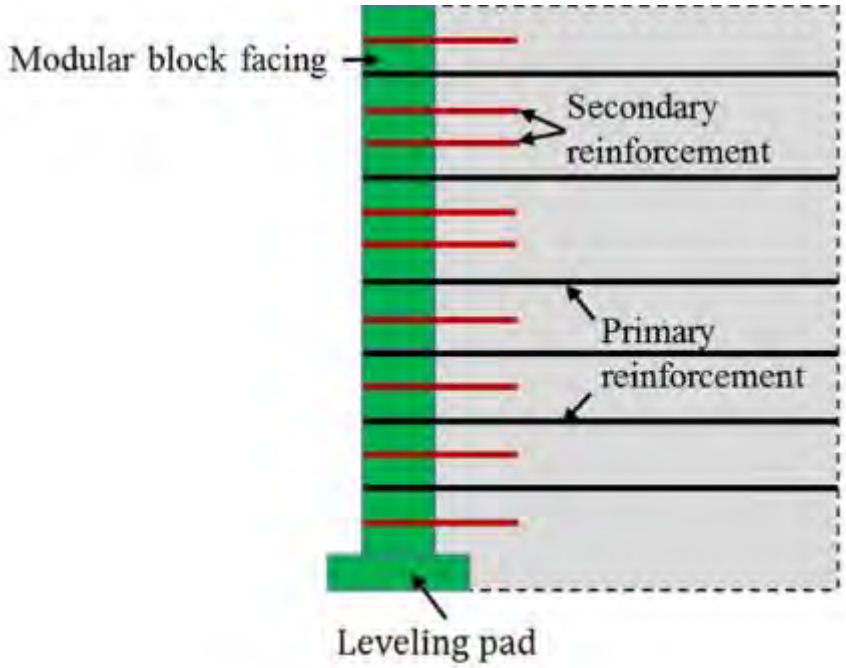

Figure 1.2: Cross Section of an MSE Wall with Secondary Reinforcements

1.3 Research Objective

The objective of this project was to evaluate the effects of secondary reinforcement on the behavior of the MSE walls and develop design guidelines to consider the effects of secondary reinforcements on connection loads and internal stability.

1.4 Research Methodology

The methodology utilized for this research includes: (1) a literature review of geosynthetic-reinforced slopes and MSE walls with secondary reinforcements and instrumentation techniques; (2) laboratory tests performed to assess the properties of materials including backfill soil, retained soil, and geogrids used in the test walls; (3) field tests to evaluate the effects of secondary reinforcement on the behavior of the MSE walls; and (4) the development of design guidelines to consider the effects of secondary reinforcements on connection loads and internal stability. The materials property tests were conducted at the

Department of Civil, Environmental, and Architectural Engineering at the University of Kansas (KU). Field tests were performed on the construction site of the I-70/K-7 interchange project in Kansas.

1.5 Report Organization

This report consists of six chapters. Following this chapter, a literature review of past studies on MSE walls is described in Chapter 2. Chapter 3 presents the test results of the materials (e.g., fill, soil, and geogrids) used in the field tests. The measured results from field tests during and after construction were analyzed and discussed in Chapter 4. Summary and conclusions are given in Chapter 5.

Chapter 2: Literature Review

In this chapter, a literature review consists of two parts. The first part focuses on the field or laboratory experimental studies on MSE walls reinforced with geosynthetics. The second part concentrates on the studies related to the geosynthetic-reinforced slopes and MSE walls with secondary reinforcements.

2.1 Literature Review of MSE Walls

Field or laboratory experimental tests have been commonly performed to evaluate the behavior of MSE walls under working and limit-state conditions. Various instrumentations, such as survey targets, inclinometer casings, earth pressure cells, telltales, and strain gauges, have been employed to monitor the performance of MSE walls. Wall facing deflections, distributions of lateral earth pressures, and distributions of tensile strains or stresses in geosynthetics are three key parameters most researchers have measured. Table 2.1 summarizes 14 field or experimental studies of MSE walls.

These MSE walls had a wrapped-around, concrete panel, or a modular block facing. Among them, most of the MSE walls had a modular block facing. The heights of these walls varied from 20 to 55.8 ft, and the lengths of geosynthetic reinforcement changed from 8.3 to 40 ft. The vertical reinforcement spacing was in the range of 1 to 3.3 ft. Eight of 14 walls had a 2-ft vertical reinforcement spacing.

Various geosynthetics, such as high-density polyethylene (HDPE) geogrids, biaxial polypropylene geogrids, and polyester geogrids, were used to reinforce the walls. Ten of 14 walls utilized HDPE geogrids. Sand, gravel, or lime-treated soil was employed as the backfill soil in these walls. Most of them were constructed on firm foundations, such as bedrock, concrete, and sandy gravel.

A large number of instrumentations were installed to monitor the performance of these MSE walls. These instrumentations included inclinometer casings, surveying targets, linear variable differential transformers (LVDTs), earth pressure cells, strain gauges, and extensometers. They could measure lateral displacements, vertical and lateral earth pressures,

and strains of geogrids. Among these instrumentations, inclinometer casings, earth pressure cells, and strain gauges were frequently used in the field and laboratory experimental tests.

2.2 Literature Review of MSE Walls with Secondary Reinforcements

Compared with traditional MSE walls, MSE walls with secondary reinforcements have been rarely investigated. Only several numerical and theoretical studies were performed on this topic. In this section, the literature regarding the geosynthetic-reinforced slopes and MSE walls with secondary reinforcements is reviewed.

Secondary reinforcement was first used to stabilize surficial slopes. Thielen and Collin (1993) conducted a detailed analysis on geosynthetic-reinforced slopes with secondary reinforcements. The function and the strength requirement of secondary reinforcements can be found in Berg (1993) and Elias and Christopher (1997), respectively. A stability analysis was performed on geosynthetic-reinforced slopes with secondary reinforcements by Michalowski (2000) based on shallow failure mechanisms. In his study, the length, spacing, and strength of secondary reinforcements were determined by utilizing the kinematic theorem of limit analysis.

Secondary reinforcement was considered for MSE walls later than that for slopes. Leshchinsky (2000) suggested the use of secondary reinforcements to mitigate the problems resulting from the large vertical spacing of primary reinforcement in MSE walls. Leshchinsky indicated that the use of secondary reinforcement in MSE walls results in the following advantages: (1) a reduction in connection loads for primary reinforcements, (2) an increase in internal stability by secondary reinforcement, (3) improved compaction near the wall facing, and (4) alleviation of down-drag behind the wall facing. Leshchinsky and Vulova (2001) employed a numerical method to investigate the influence of secondary reinforcements on the performance of MSE walls. Their study illustrated that the inclusion of secondary reinforcement could reduce the connection loads of primary reinforcement, increase wall internal stability, and change the failure mode from connection failure to compound failure. Han and Leshchinsky (2006) and Leshchinsky, Kang, Han, and Ling (2014) used the limit equilibrium method to investigate the effects of secondary reinforcements on the behavior of MSE walls. They demonstrated that the use of secondary reinforcements could reduce connection loads.

Table 2.1: Summary of Field or Laboratory Experimental Tests of MSE Walls

No.	1	2	3	4	5	6	7
Authors	Allen, Christopher, and Holtz	Ling and Leshchinsky	Bathurst, Walters, Vlachopoulos, Burgess, and Allen	Bathurst, Walters, Vlachopoulos, Burgess, and Allen	Abu-Hejleh, Zornberg, Wang, McMullen, and Outcalt	Yoo and Jung	Yoo
Year	1992	1996	2000	2000	2001	2004	2004
Location	Seattle, Washington, U.S.	Stockbridge, Georgia, U.S.	Royal Military College, Canada	Royal Military College, Canada	Founder/Meadows, Colorado, U.S.	None	Korea
Wall facing	Wrapped-around	Modular block	Modular block	Wrap-round	Modular block	Modular block	Modular block
Wall height (ft)	39.4	22.4	11.8	11.8	14.8-19.4	16.4	27.6
Reinforcement length (ft)	39.4	6.6	8.3	8.3	>26.2	11.5	20.7
Reinforcement spacing (ft)	1.2	1.3-2.6	2.0	2.0	1.3	1.0-2.0	1.3-3.3
Geosynthetics type	Polyester and polypropylene geogrids	HDPE geogrids	Biaxial polypropylene geogrids	HDPE geogrids	Geogrids	Polyester geogrids	HDPE geogrid
Backfill material	Subangular gravelly sand	Sand	Rounded beach sand	Rounded beach sand	Gravel+sand+fine grained soil	Well-graded silty sand	Poorly-graded sand
Foundation	Unknown	Sand	Concrete	Concrete	Bedrock	Unknown	Unknown
Instrumentation	Inclinometers, earth pressure cells, strain gauges, mechanical extensometers, settlement targets, weather station	Inclinometers, earth pressure cells, and strain gauges	Facing potentiometers, earth pressure cells, and strain gauges, extensometer, settlement plate	Facing potentiometers, earth pressure cells, and strain gauges, extensometer, settlement plate	Inclinometers, survey targets, earth pressure cells, and strain gauges, moisture gages, and temperature gages	LVDTs and strain gauges	Surveying targets
Measurements	Lateral displacements, vertical earth pressures, strains of soil, strains of geotextiles, settlements	Lateral displacements, lateral earth pressures, and strains of geogrids	Lateral displacements, lateral earth pressures, and strains of geogrids	Lateral displacements, lateral earth pressures, and strains of geogrids	Lateral displacements, stains of geogrids, temperatures, and vertical earth pressures	Lateral displacements and stains of geogrids	Lateral displacements

Table 2.1: Summary of Field or Laboratory Experimental Tests of MSE Walls (Continued)

No.	8	9	10	11	12	13	14
Authors	Desai and El-Hoseiny	Yang, Zhang, Lv, and Zhou	Yang, Ding, Zhou, and Zhang	Pierson, Parsons, Han, and Brennan	Yang, Liu, Lv, and Zhang	Allen and Bathurst	Yang, Liu, Zhou, and Xiong
Year	2005	2009	2010	2011	2012	2013	2014
Location	Tanque Verde, Arizona, U.S.	Fujian, China	Fujian, China	Kansas, U.S.	Heibei, China	Maple Valley, Washington, U.S.	Shangdong, China
Wall facing	Concrete panel	Geotextile gravel bag+Concrete	Geotextile gravel bag	Modular block	Modular block	Modular block	Modular block
Wall height (ft)	15.7	40.0	40.0	19.7	19.7	20.7	55.8
Reinforcement length (ft)	12.1	24.6	24.6	13.8	16.4	25.9	6.6
Reinforcement spacing (ft)	1.3-2.6	1.3-1.7	1.3-2.0	2.0	1.3-2.0	2.0	1.0-2.0
Geosynthetics type	HDPE geogrid	HDPE geogrid	HDPE geogrid	HDPE geogrid	HDPE geogrid	HDPE geogrid	HDPE geogrid
Backfill material	Unknown	Rammed clay+Reclaimed gravel soil	Rammed clay+Reclaimed gravel soil	Aggregates	Lime-treated soil	Well-graded silty gravelly sand	Soil-rock mixture
Foundation	Unknown	Gravel soil	Gravel soil	Bedrock	Sandy gravel	Dense silty sandy gravel	Bedrock
Instrumentation	Stain gauges, earth pressure cells, induction coils, and temperature gages	Inclinometers, surveying targets, earth pressure cells, and strain gauges	Inclinometers, surveying targets, earth pressure cells, and strain gauges	Inclinometers, earth pressure cells, and strain gauges	Inclinometers, earth pressure cells, and strain gauges	Stain gauges, extensometers, temperature gages	Surveying target, earth pressure cells, and strain gauges
Measurements	Stains of geogrids, vertical earth pressures, and temperatures	Lateral displacements, vertical and lateral earth pressures, and strains of geogrids	Lateral displacements, vertical and lateral earth pressures, and strains of geogrids	Lateral displacements, lateral earth pressures, and strains of geogrids	Lateral displacements, lateral earth pressures, and strains of geogrids	Stains of geogrids and temperatures	Lateral displacements, lateral earth pressures, and strains of geogrids

Chapter 3: Material Properties

In this chapter, tests were performed to obtain the physical and mechanical properties of the materials used in the test walls. The tested materials included backfill soil, retained soil, and geogrids.

3.1 Backfill Soil

The backfill soil used in the field MSE wall was aggregates. The aggregates were produced by a local quarry in Bonner Springs, KS. Representative aggregates were taken from the test site. The tests conducted in the laboratory and field were sieve analysis tests, standard Proctor tests, sand cone tests, plate loading tests, and triaxial shear tests.

3.1.1 Sieve Analysis Tests

Sieve analysis tests were performed in the laboratory to determine the particle size distribution of the aggregate for the backfill soil. These sieve analysis tests followed the ASTM C136 (2006) standard. Figure 3.1 shows the particle size distributions of this aggregate. The particle size distributions of the aggregate were within the upper and lower bounds.

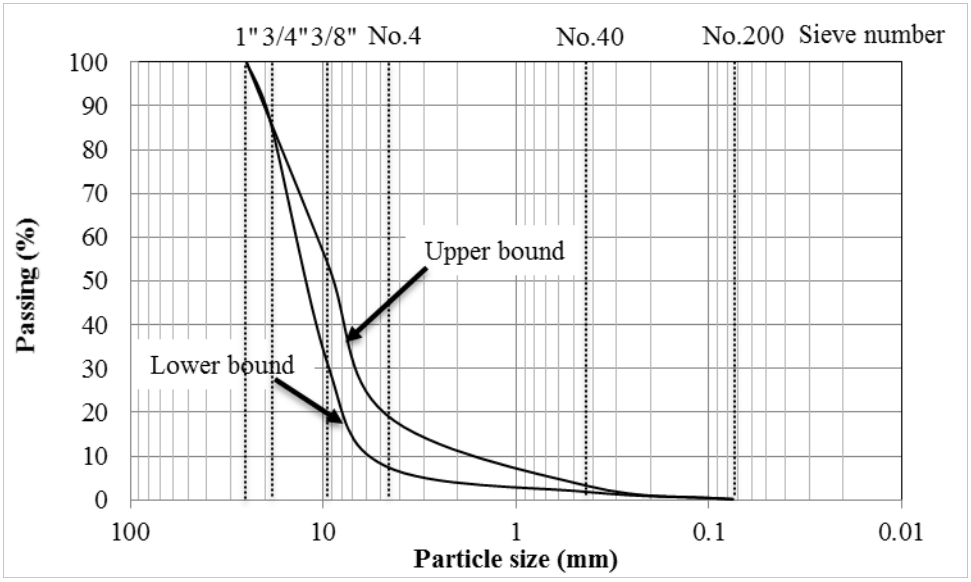

Figure 3.1: Particle Size Distribution of the Backfill Soil

3.1.2 Standard Proctor Tests

Standard Proctor tests were performed to obtain the maximum dry unit weight and its corresponding optimum moisture content of the aggregate. According to the particle size distribution of the aggregate, less than 30% particles of the aggregate was retained on the 3/4" sieve. Therefore, Method C in the ASTM D698 (2012) standard was adopted. Figure 3.2 shows the compaction curve of this aggregate. The maximum dry unit weight of the aggregate was 106.8 pcf and its corresponding optimum water content was 2.65%.

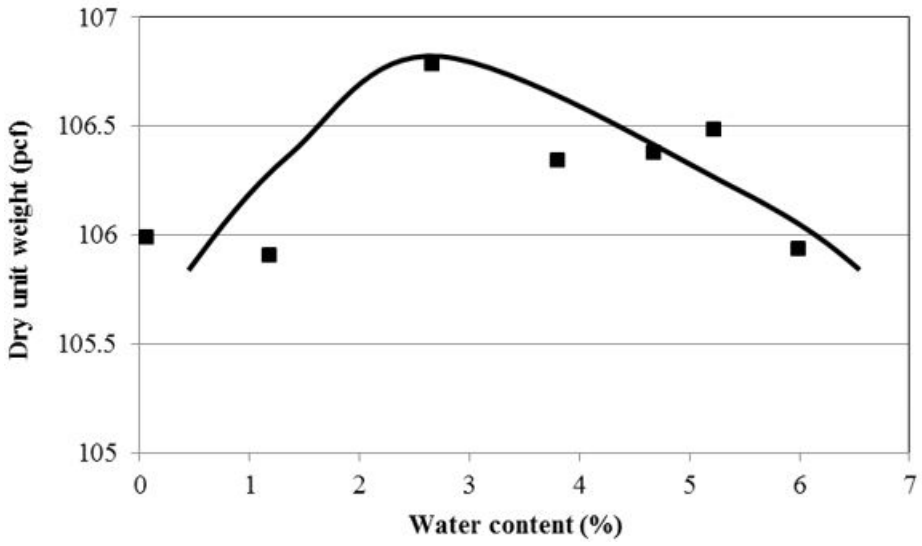

Figure 3.2: Results of Standard Proctor Tests

3.1.3 Sand Cone Tests

During construction, two types of equipment were used to compact the aggregate. One was a roller compactor and the other one was a light-weight plate compactor, as shown in Figure 3.3. The light-weight plate compactor was used to compact the aggregate within 3 ft behind the back of wall facing, while the roller compactor was used to compact the aggregate at 3 ft away from the back of wall facing.

Sand cone tests were performed at selected locations in these two areas. The procedures of sand cone tests followed the ASTM D1556 (2007) standard. Additionally, in each sand cone test, a piece of thin plastic wrap was placed and fully in contact with the top surface of

aggregates. This piece of thin plastic wrap was used to prevent loss of sand into aggregates. Four sand cone tests were conducted in the area within 3 ft behind the back of wall facing, while eight sand cone tests were conducted in the area at 3 ft away from the back of wall facing. Figure 3.4 shows the operation of sand tests at two different compaction areas in the field. The average most density of the aggregate was 114.8 pcf and its corresponding average moisture content was 3.1%; therefore, the average unit weight of the aggregate was 111.4 pcf. In addition, the relative compaction of aggregate was more than 95%.

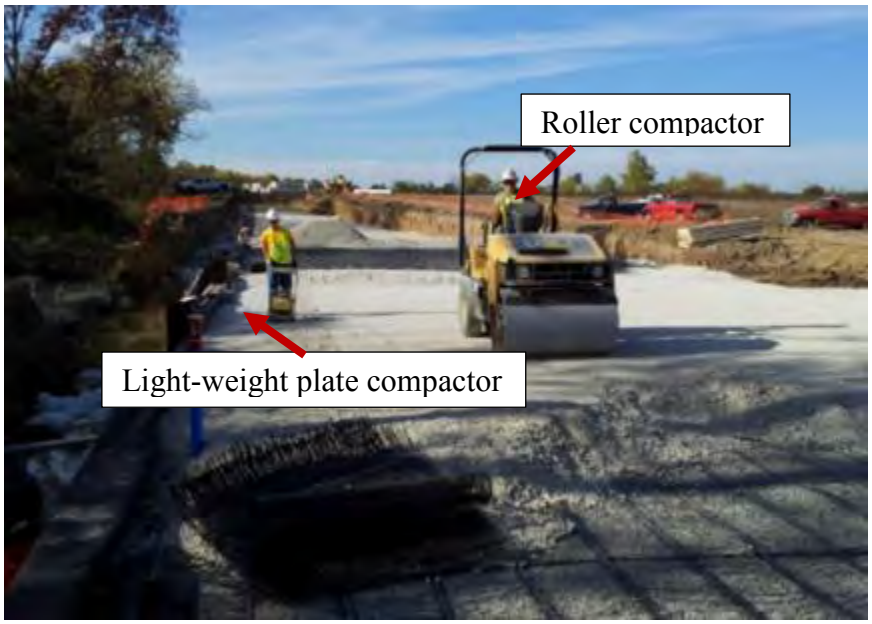

Figure 3.3: Roller Compactor and Light-Weight Plate Compactor

(a) The area within 3 ft behind the back of wall facing

(b) The area at 3 ft away from the back of wall facing

Figure 3.4: Sand Cone Tests in the Field

3.1.4 Plate Loading Tests

Plate loading tests were conducted in the laboratory to obtain the load-displacement curves of the aggregate, which would be used to calibrate the elastic modulus of the aggregate in numerical study. Figure 3.5 shows the setup of one plate loading test. The equipment of the plate loading test included a wood box, a reaction frame, an air cylinder, and a circular loading plate. The dimension of the wood box was 24 inches in length, 24 inches in width, and 20 inches in height. The diameter of the loading plate was 6 inches. In addition, the thickness of the compacted aggregate underneath the loading plate in the wood box was 16 inches. The length and width of the wood box were 4 times larger than the diameter of the loading plate, while the thickness of the aggregate was 4 times larger than the diameter of the loading plate. As a result, the boundary effect was minimized.

In order to find the relationship between the unit weight and the modulus of the aggregate, three plate loading tests were performed on the aggregate at three different unit weights. The aggregate was compacted in the wood box with three lifts. Each lift did not exceed 8 inches. An air hammer compactor was employed to compact the aggregate to the desired density with a level surface. A less than 0.5-inch layer of sand was placed on the top surface of the aggregate underneath the loading plate. After that, loads were applied in increments on the aggregate until the aggregate failed or the 105-psi loading capacity of the air cylinder was reached. At each load increment, a stable settlement and its corresponding load were recorded for the load-displacement curve. The detailed procedures of the plate loading test followed the ASTM D1196 (2012) standard.

Figure 3.6 shows the load-displacement curves of the aggregate at three unit weights. The aggregate at a higher unit weight had less settlement at the same load. In other words, the aggregate at a higher unit weight had a higher elastic modulus. Equation 3.1 was used to calculate the elastic modulus of the aggregate based on the linear portion of the load-displacement relationship:

$$E = \frac{qB\left(1-\upsilon^2\right)}{s} I_f$$ **Equation 3.1**

Where:

E = elastic modulus

q = applied pressure on the aggregate

B = width of the loading plate

υ = Poisson's ratio

s = displacement

I_f = influence factor for the circular loading plate

Figure 3.7 shows that the modulus of the aggregate had a good linear relationship with the density.

Figure 3.5: The Setup of a Plate Loading Test

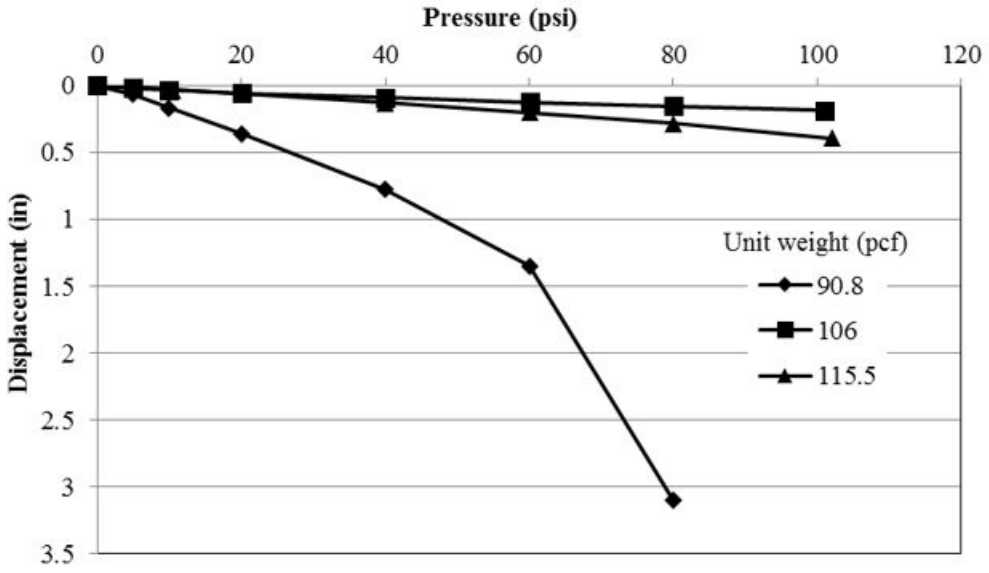

Figure 3.6: Load-Displacement Relationship of the Aggregate with Three Compaction Unit Weights

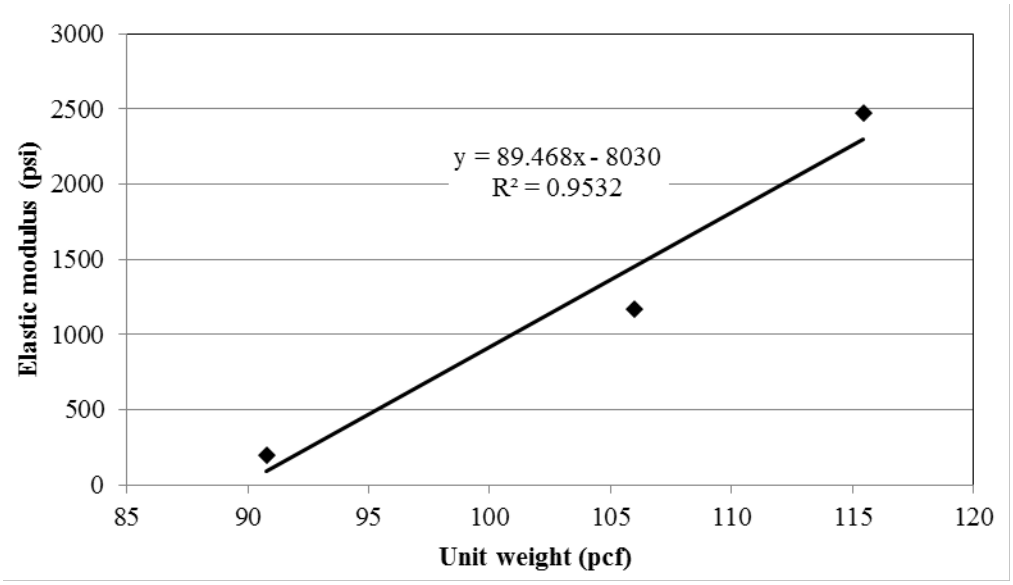

Figure 3.7: Relationship Between Modulus and Unit Weight of the Aggregate

3.1.5 Triaxial Shear Tests

Triaxial shear tests were performed to obtain stress-strain relationships and shear strengths of the aggregate. According to the maximum particle size of the aggregate, the aggregate samples with a diameter of 4 inches and a height of 8 inches were prepared in the tests to minimize the boundary effect. Figure 3.8 shows the setup of a triaxial shear test. The tests

were conducted at three confining stresses to obtain a Mohr-Coulomb envelope. The confining stresses of 7.3, 14.5, and 29 psi were selected and applied to the samples to simulate the overburden stresses of the aggregate at three depths in the field. The confining stress was applied after the sample was saturated. Each sample was tested under a drained condition. In addition to the strain and stress measured in the test, the volume change of the sample was measured. The procedures for triaxial shear tests were in accordance with the ASTM D7181 (2011) standard.

Figures 3.9(a) and (b) show the stress-strain relationships and the axial-volumetric strain relationships of the aggregate at three confining stresses, respectively. Figure 3.9(a) shows that the strains at three confining stresses gradually increased with an increase of the deviatoric stresses until the sample reached the critical state. The peak friction angle of the aggregate, ϕ_{peak} = 47°. In addition, the aggregate had the dilative behavior under the confining stresses of 7.3 and 14.5 psi.

Figure 3.8: Setup of a Triaxial Shear Test

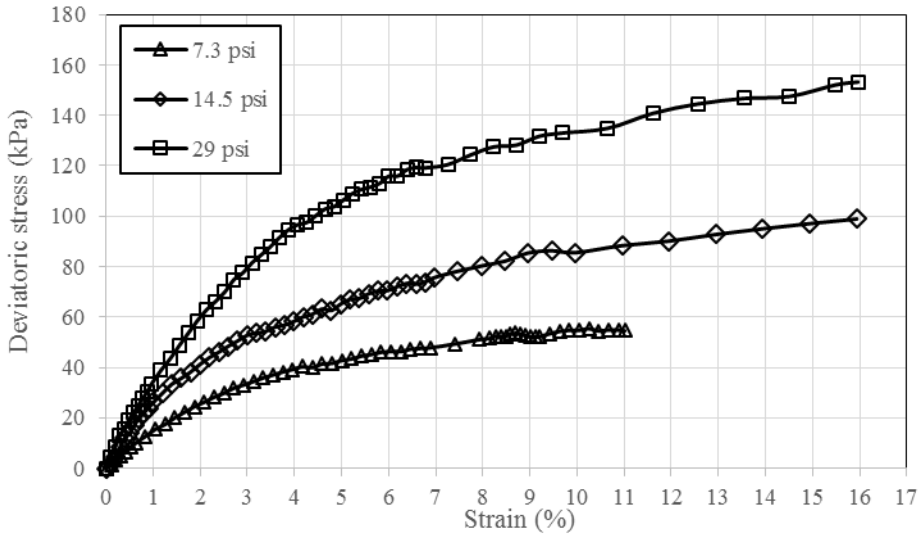

(a) Stress-strain relationships

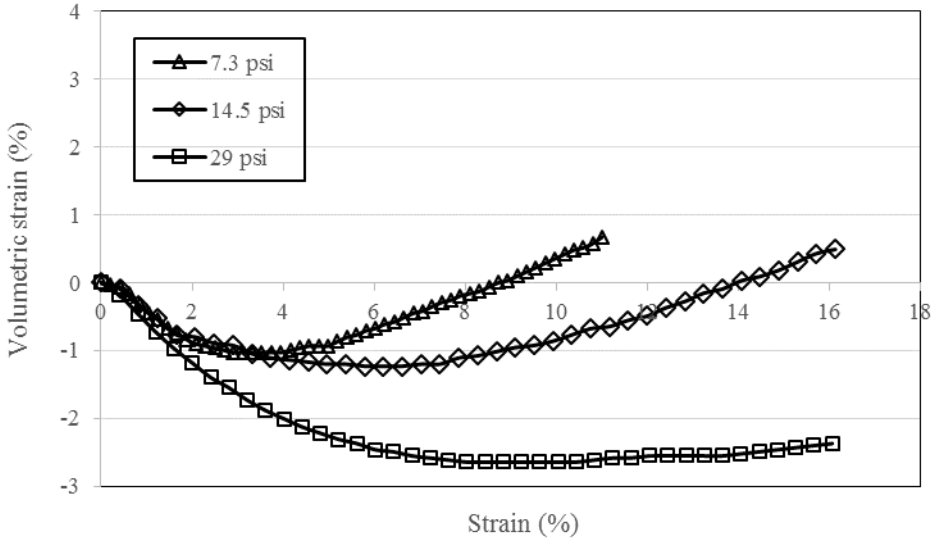

(b) Axial-volumetric strain relationships

Figure 3.9: Triaxial Shear Test Results of the Aggregate

3.2 Retained Soil

The retained soil in the field test was a borrow soil. This soil was obtained from a site nearby the field test site. Atterberg limit and sand cone tests were conducted in the laboratory and in the field, respectively, to obtain the physical properties of the retained soil.

3.2.1 Atterberg Limit Tests

Atterberg limit tests were conducted to obtain the plastic limit (PL) and liquid limit (LL) of the retained soil. The retained soil was first dried in an oven at 110° for 24 hours. The dry soil was smashed and ground. This ground soil that passed a No. 40 sieve was kept to carry out the Atterberg limit tests. The test procedures for PL and LL followed the ASTM D4318 (2010) standard. The measured LL and PL of the retained soil were 42 and 20, respectively. The plastic index was calculated to be 22 based on Equation 3.2:

$$PI = LL - PL \qquad \textbf{Equation 3.2}$$

According to the plasticity chart (shown in Figure 3.10), the retained soil is classified as CL. Furthermore, the shrinkage limit of the retained soil was 15 according to ASTM D2487 (2011).

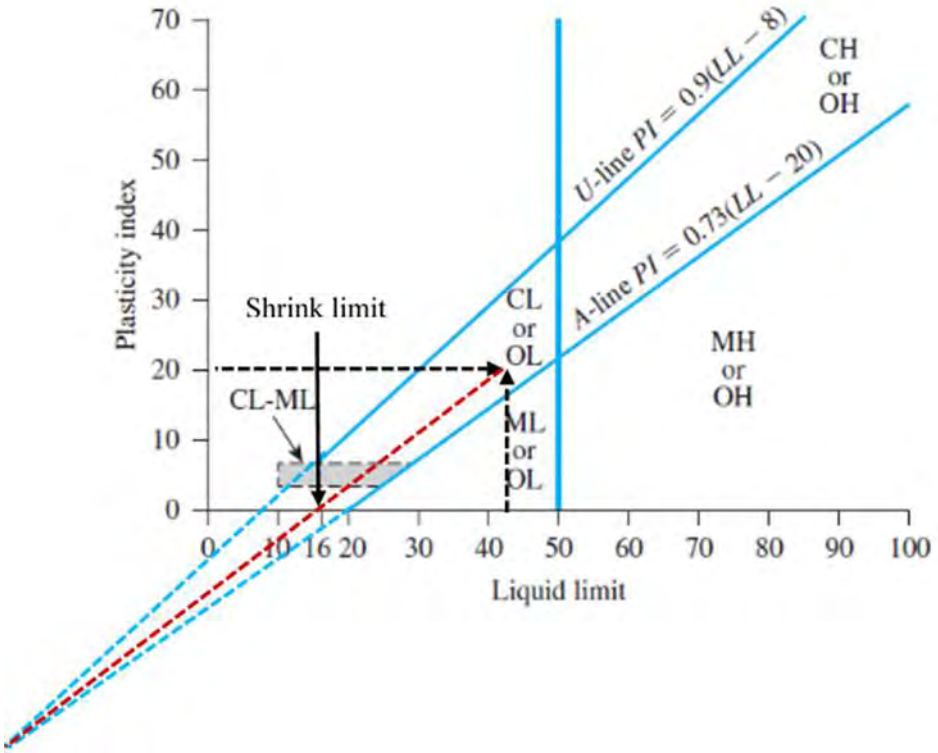

Figure 3.10: Plasticity Chart
Modified from ASTM D2487 (2011) Standard

3.2.2 Sand Cone Tests

The retained soil was compacted by a sheep foot roller in the field. Sand cone tests were carried out to measure the unit weight of the compacted retained soil. The procedures of the sand cone tests were consistent with the ASTM D1556 (2007) standard. The moist unit weight of the retained soil was 127 pcf and its corresponding moisture content was 21%. The dry unit weight of the retained soil was 105 pcf.

3.3 Geogrids

Five types of geogrids were used in the field test as reinforcements. Four of them were uniaxial (UX) HDPE geogrids and one of them was biaxial (BX) polyethylene geogrid. The pictures of UX and BX geogrids are shown in Figures 3.11(a) and (b), respectively. The physical and mechanical properties of the geogrids provided by the manufacturer are shown in Table 3.1. The following properties of BX geogrids are presented in the cross-machine direction (XMD): initial modulus = 400 kN/m, tensile strength at 2% strain = 6.6 kN/m, and junction efficiency = 93%.

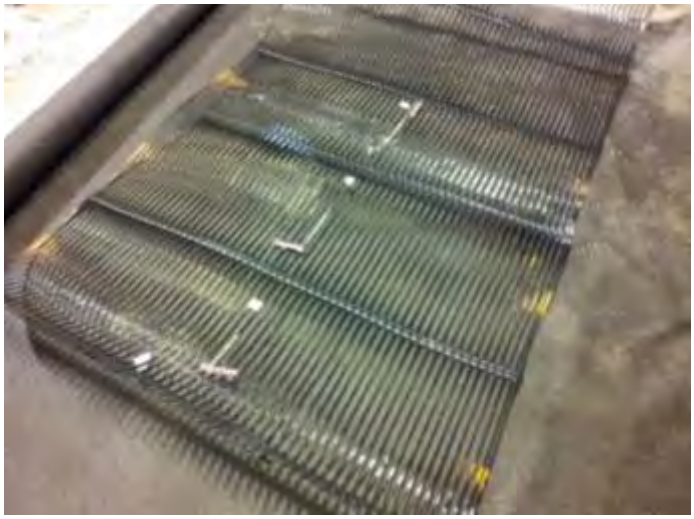

(a) Uniaxial geogrid

Figure 3.11: Two Types of Geogrids

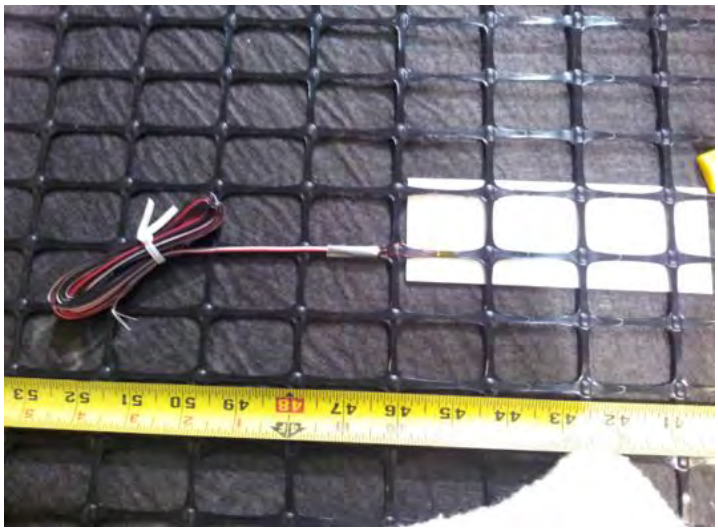

(b) Biaxial geogrid

Figure 3.11: Two Types of Geogrids (Continued)

Table 3.1: Properties of Geogrids (Provided by Manufacturer)

Property	UX1	UX2	UX3	UX4
Ultimate tensile strength (lb/ft)	3970	4800	7810	9870
Maximum allowable (design) strength for 120-year design life (lb/ft)	1450	1760	2860	3620
Reduction factor for installation damage RF_{ID}	1.05			
Reduction factor for creep RF_{CR}	2.6			
Reduction factor for durability RF_{D}	1.0			

3.3.1 Tests for Global Strain and Local Strain Relationships

In the field test, strain gauges were attached on the geogrids to measure strains of geogrids. Perkins, Schulz, and Lapeyre (1997) and Bathurst, Allen, and Walters (2002) found that the measured local strains on a geogrid by strain gauges might be different from the global strains of the geogrid because of the geogrid apertures. The difference between local and global strains depends on geogrid type.

Laboratory tests were conducted to establish the relationships between local and global strains of the geogrids used in this study. Figure 3.12 shows the setup of the test. The procedures of the ASTM D6637 (2015) standard that is used to measure the tensile strength of geogrids were adopted to conduct this test. Figure 3.13 shows the relationships of the local and global strains of the geogrids. A calibration factor (CF) was used to describe the relationship, which is defined as the ratio of global strain to local strain. The global strains linearly increased with the local strains at the beginning. However, the global strains increased dramatically when the local strains approached to 2%, because the attached strain gauges were debonded from the geogrids. Therefore, the CF was computed based on the linear portion, which was prior to the debonding of strain gauges from the geogrids. The CFs for primary and secondary reinforcements ranged from 1.00 to 1.29. In addition, Figure 3.14 shows the tensile stress-strain relationships of all the geogrids used in this study. The global strains of the geogrids increased nonlinearly with the tensile stresses. Under the same tensile stress, the induced global strains of the geogrids from the maximum to the minimum were BX, UX1, UX2, UX3, and UX4. These results are consistent with the properties of the geogrids provided by the manufacturer.

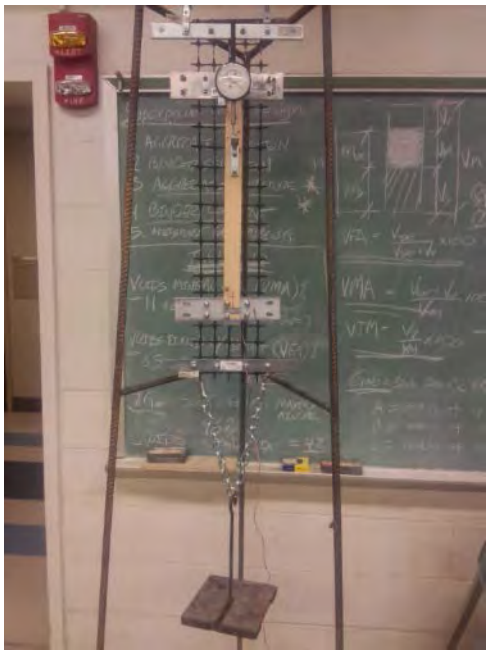

Figure 3.12: Test Setup for Local and Global Strains of Geogrids

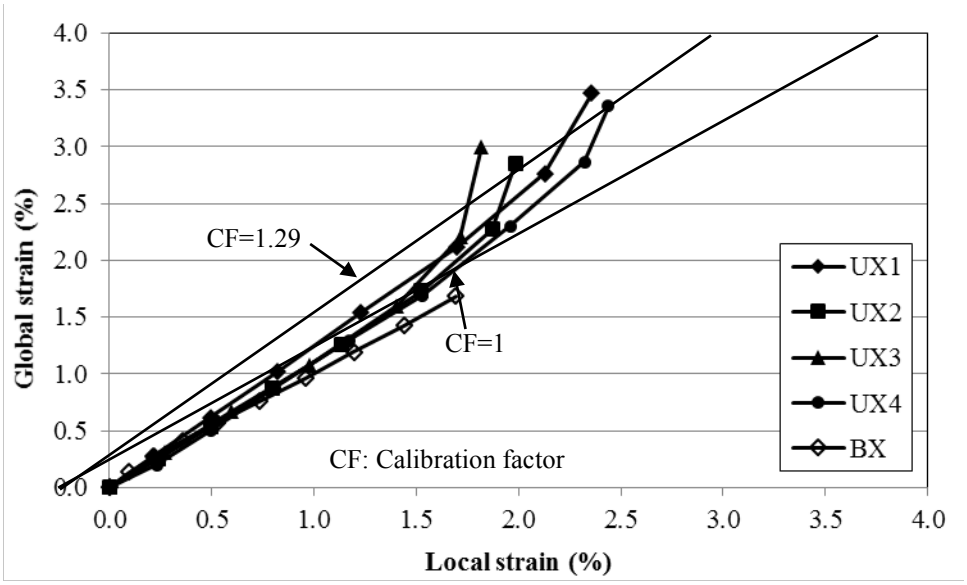

Figure 3.13: Relationships of Local and Global Strains of Geogrids

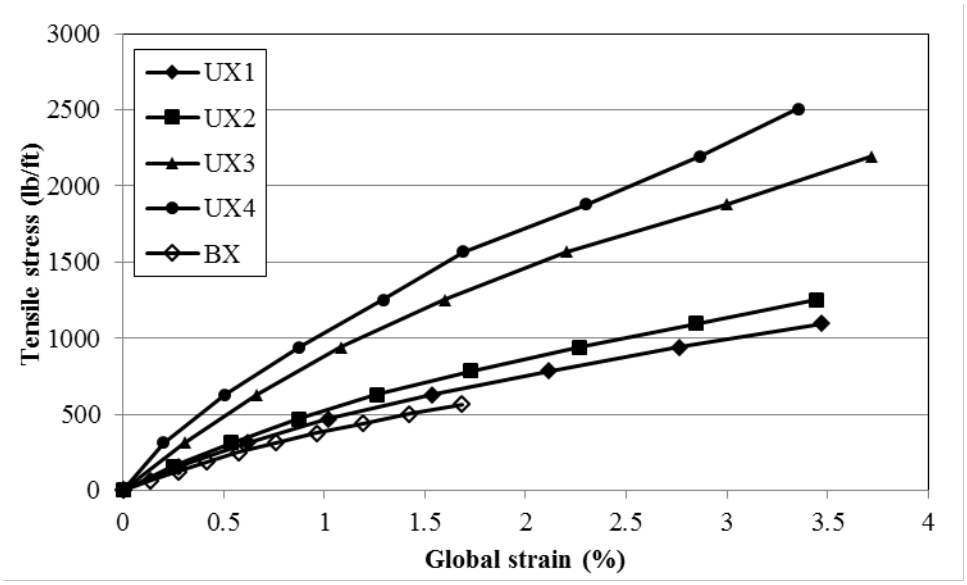

Figure 3.14: Tensile Stress-Strain Relationships of Geogrids

Chapter 4: Field Tests of MSE Walls with Secondary Reinforcements

4.1 Project Background

The test walls were located in Bonner Springs, Wyandotte County, KS, which were constructed to retain a new ramp in the Kansas Department of Transportation I-70/K-7 interchange project. Figure 4.1 shows the plan view of the project.

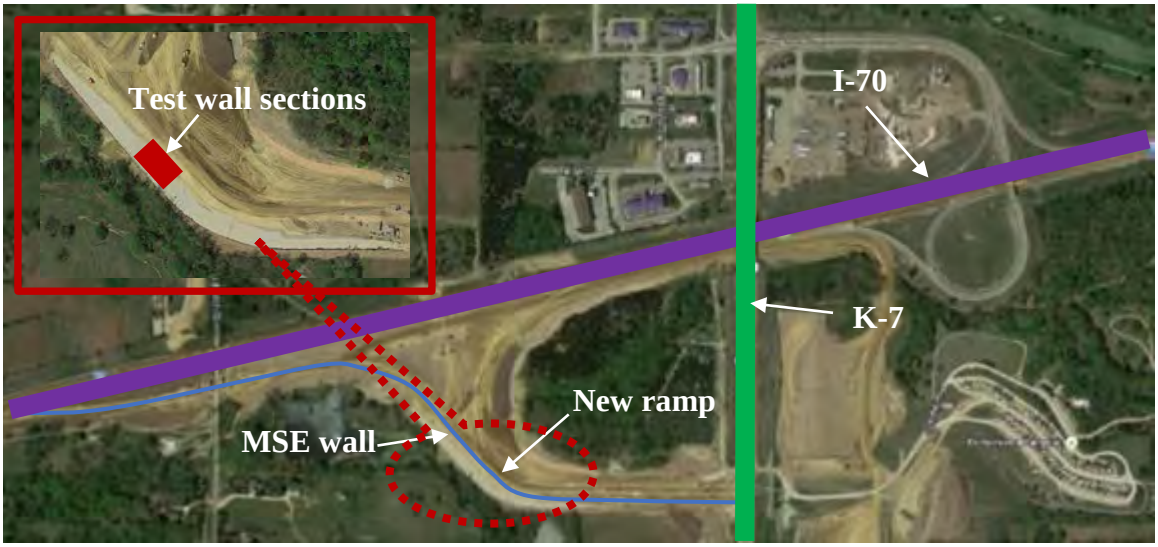

Figure 4.1: Location of Three Test Wall Sections
Source: Google (n.d.)

4.2 Test Wall Sections

Three test wall sections were monitored. Separators were installed to isolate test wall sections between each other. Figure 4.2 presents the front view of these test wall sections. The test wall sections had a width ranging from 33.5 to 37.0 ft and a height ranging from 37.6 to 39.0 ft.

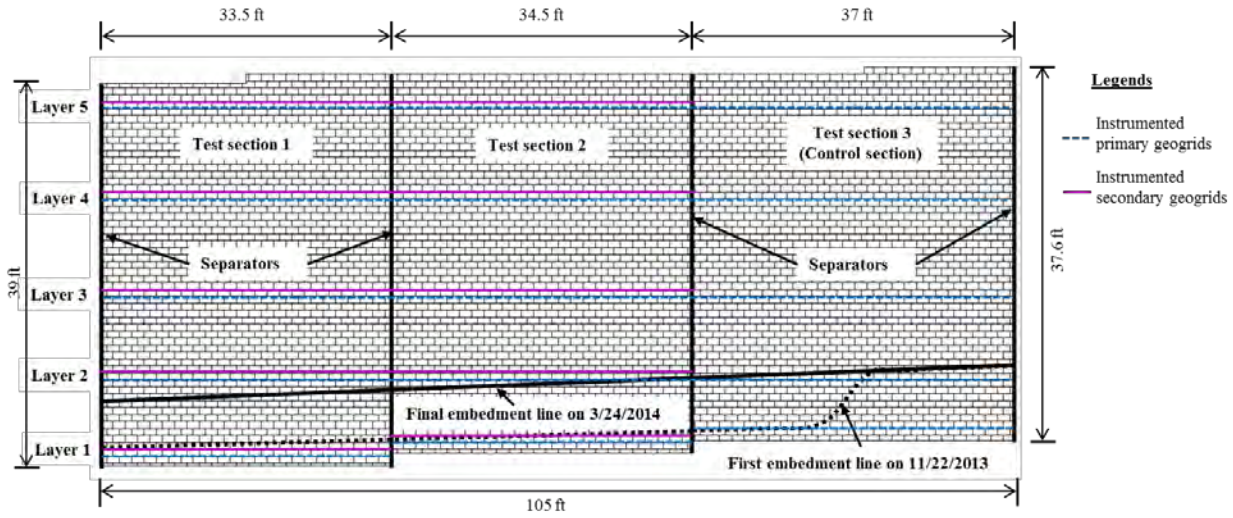

(a) Illustration (not to scale)

(b) Photo

Figure 4.2: Front View of Three Test Wall Sections

Figure 4.3 shows the layouts of primary and secondary reinforcements in the test wall sections. Test Section 1 (TS1) had uniaxial geogrids as primary and secondary reinforcements. Test Section 2 (TS2) had uniaxial geogrids as primary reinforcements and biaxial geogrids as secondary reinforcements. Test Section 3 (TS3) had uniaxial geogrids as primary reinforcements

without any secondary reinforcement, which was the control section. The lengths of primary reinforcements in TS1, TS2, and TS3 were 61 to 62 ft, 60 to 61 ft, and 58 to 59 ft, respectively. The ratios of the primary reinforcement length to the wall height for all three test wall sections were approximately 1.6. This ratio was about 2 times greater than the recommended ratio of 0.7 by Elias and Christopher (1997). The primary reinforcements were placed every two blocks (i.e., 16 inches) in the one-third lower part of the test wall sections and placed every three blocks (i.e., 24 inches) in the two-third upper part of the test wall sections. The secondary reinforcements in TS1 were 6 ft long (4.5 ft without including the tails) and placed between two primary reinforcements. Similarly, the secondary reinforcements in TS2 were 4.3 ft long and placed between two primary reinforcements. The coverage ratio of either primary or secondary reinforcements in three test wall sections was 100 percent.

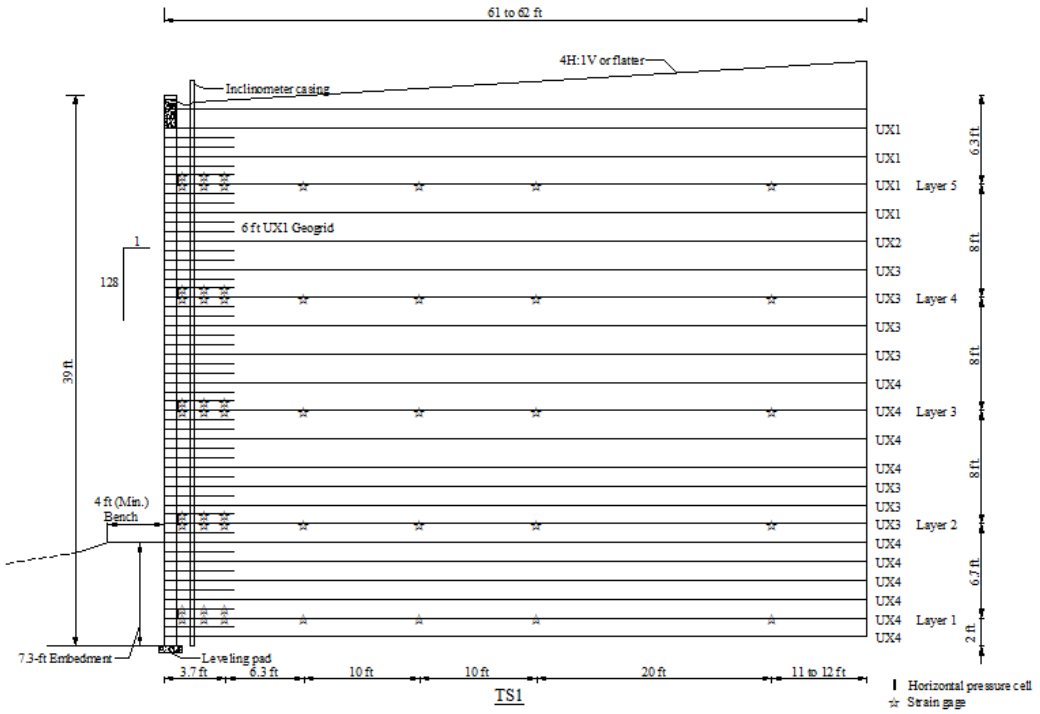

(a) TS1

Figure 4.3: Cross Sections of Three Test Wall Sections with Instrumentation (Not to Scale)

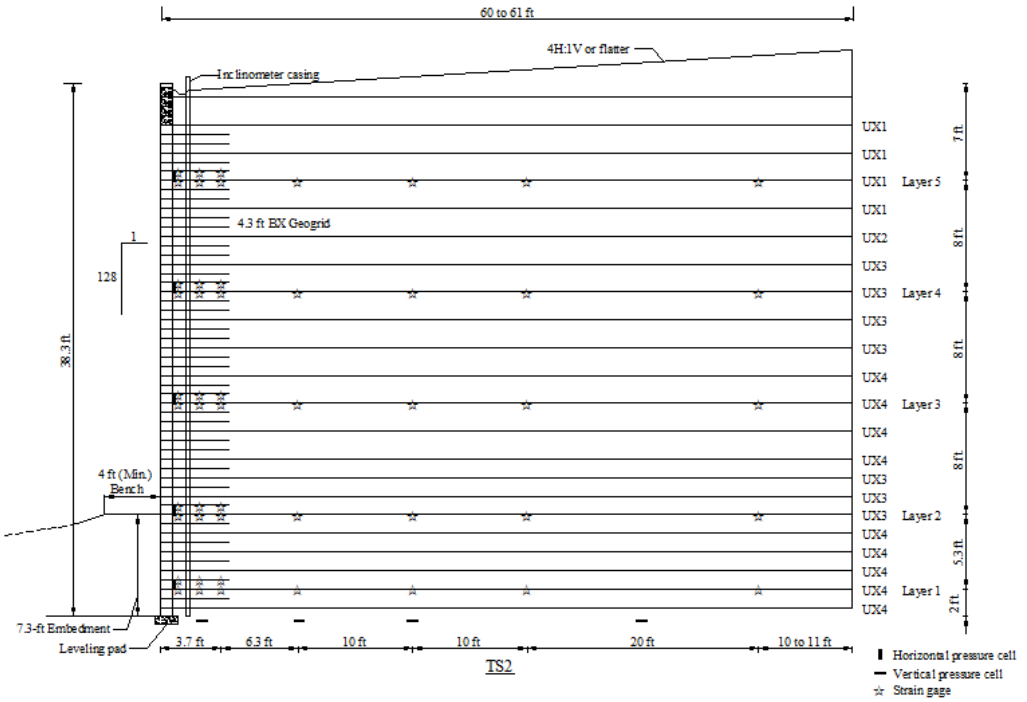

(b) TS2

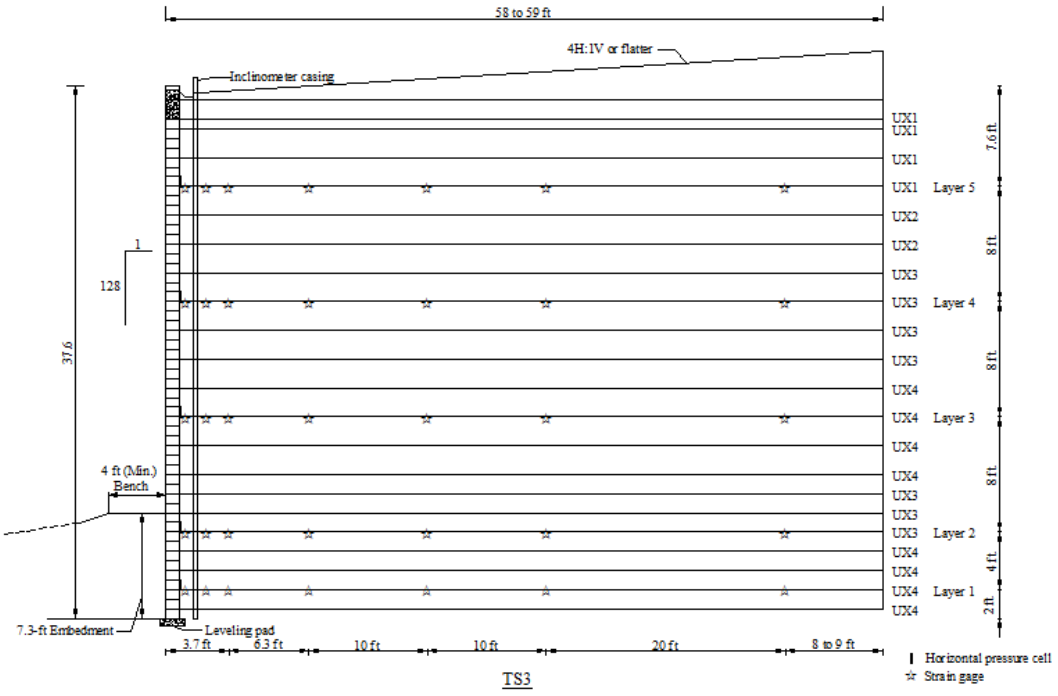

(c) TS3

Figure 4.3: Cross Sections of Three Test Wall Sections with Instrumentation (Not to Scale) (Continued)

4.3 Test Wall Design

All the test wall sections were designed by the third party based on the MSE wall reinforced with primary reinforcements only (i.e., the control section). The design used the Load and Resistance Factor Design (LRFD) method that was included in the AASHTO (2007) design guideline. In this study, a software of MSEW (3.0) was employed to examine the design of the test wall sections. The MSEW (3.0) was an updated version of MSEW (1.0) that was developed for the FHWA and widely used for the design of MSE walls in North America. The MSEW (3.0) not only incorporated the AASHTO 2007 and 2010 LRFD method but also included the AASHTO 98 Allowable Stress Design (ASD) method, the AASHTO 2002 ASD method, and the NCMA design method.

The parameters used in the Class A design of three test wall sections were determined before the construction. The selection of these parameters was in accordance with AASHTO (2007). After the construction of the test wall sections, laboratory tests were performed on the backfill soil to determine parameters used in the Class C design. Table 4.1 summarizes the soil parameters used in the wall design. The settlements of the test wall sections were ignored because they were built on bedrock. The Capacity Demand Ratios (CDRs) for external and internal stability in the Class A and C designs are summarized in Table 4.2. The CDRs for external stability in the Class C design were the same as those in the Class A design because the friction angle of retained soil used in the Class C design was the same as that in the Class A design. The CDRs for internal stability in the Class C design were much larger than those in the Class A design because the friction angle of the backfill soil used in the Class C design was larger than that in the Class A design, which dramatically reduced the lateral earth pressures.

Table 4.1: Soil Parameters Used in the Design of Test Wall Sections

Properties	Class A[2]			Class C[3]		
	Unit weight (pcf)	Friction angle (°)	Cohesion (psi)	Unit weight (pcf)	Friction angle (°)	Cohesion (psi)
Backfill soil	120.3	34	0	114.8	47	0
Retained soil	129.3	25	0	127.3	25	0
Foundation soil	129.9	0	145	129.9	0	145

Note: [1] The foundation of the test wall sections during construction was confirmed to be limestone and sandstone, and the cohesion of the foundation soils was assumed to be 145 psi in the design; [2] Class A represented the prediction type before the construction; [3] Class C represented the prediction type after the construction.

Table 4.2: Capacity Demanding Ratios (CDRs) in the Design of Test Wall Sections

Stability		Loading factor	Resistance factor	CDR-Class A			CDR-Class C		
				TS1	TS2	TS3	TS1	TS2	TS3
External stability	Base sliding	1	1	1.6	1.6	1.3	1.6	1.6	1.3
	Overturning	N/A	N/A	5.3	5.3	5.4	5.3	5.3	5.4
	Bearing capacity	1.35	0.65	8.3	8.4	8.8	8.3	8.4	8.8
	Eccentricity e/L[2]	1	1	0.04	0.04	0.04	0.04	0.04	0.04
Internal stability[1]	Rupture	1.35	0.9	1	1	1.1	1.9	1.7	1.9
	Pullout	1.35	0.9	49	45	53	166	140	158
	Connection	1.35	0.9	1	1	1	1.7	1.6	1.9

Note: [1] Only minimum CDRs were shown in the table; [2] The requirement for eccentricity is e/L<0.25.

4.4 Test Wall Construction

The construction of the test walls started in October 2013 and was completed in September 2014, lasting about 11 months. The test wall sections consisted of a leveling pad, modular blocks, geogrid reinforcements, a geotextile drainage, reinforced backfill, and retained

soil. Figure 4.4 illustrates the main construction steps of the test walls. The concrete leveling pad was cast in situ on the foundation to meet the grade and elevation requirements. Modular blocks were placed, spaced, and leveled accurately. Horizontal and vertical alignments of wall facing were examined about every 50 ft and 4 ft, respectively. The primary geogrids and secondary geogrids were placed as illustrated in Figures 4.4(b) and (c), respectively. The connections between primary reinforcements and wall facing, and secondary reinforcements and wall facing were mechanical connectors. Pre-tension by hand was performed on primary geogrids and secondary geogrids to mitigate the slack before aggregates were placed on the top of them. The aggregate was placed at a lift of approximately 10 inches. A roller compactor was used to compact the aggregate at 3 ft away from the back of wall facing with four to six passes, while a vibratory plate compactor was used to compact the aggregate within 3 ft of the back of wall facing. Approximately 4-inch-high concrete cap blocks were installed on the top as a protective course. Slip joints were set between test wall sections to reduce the interaction between two test wall sections. Blocks and geogrids were cut at each slip joint so that aggregate interlock became the only medium of force transmission between two MSE wall sections. The embedment of the test wall sections were constructed at two different times as shown in Figure 4.2(a). The control section (i.e., TS3) had more embedment compared with the other two test sections after the first completion of embedment. It resulted in more passive resistance effect in the control section than those in TS1 and TS2. The three test wall sections had an approximate 7.3-ft embedment depth after all the soils were placed in front of the wall.

(a) Leveling pad

(b) Installation of primary geogrids

(c) Installation of secondary geogrids

(d) Backfill material

(e) Compaction

(f) Wall capping

Figure 4.4: Construction Steps of the MSE Walls

4.5 Instrumentation Preparation and Installation

4.5.1 Inclinometers

An inclinometer casing was installed in each test wall section to measure wall facing deflections. The inclinometer system mainly consisted of inclinometer casings, an inclinometer probe with a control cable, and an inclinometer data recorder. Inclinometer casings (3.3 inches in diameter and 10 ft in length for each segment) were used in the test wall. The location of the inclinometer casing for each test section was approximately 0.6 to 1.2 ft behind the back of wall facing. A borehole was drilled into the bedrock at least 1.7 ft deep for an inclinometer casing installation at each test wall section prior to construction. Figure 4.5 shows the installation of an inclinometer casing. The inclinometer casing was lowered to the bottom of the borehole with an attached bottom cap preventing the entry of mud and water. One set of grooves inside the casing were aligned perpendicularly to wall facing before the grout was cast into the borehole to fix the casing. The grout was cast and allowed to cure before the construction of the wall. Since the bottom of the casing was fixed into the bedrock, it is reasonable to assume that the bottom of the casing did not have any deflection. The height of the inclinometer casing above the ground was measured in each test section to determine the depth of the inclinometer casing lowered in the borehole. An inclinometer probe with a more than 100-ft-long control cable and a wireless data recorder were used to collect the data for wall facing deflections in each test wall section. The inclinometer casing was timely spliced for extension according to wall height during construction.

(a) Drilling a borehole

(b) Casing installation

Figure 4.5: Inclinometer Installation

4.5.2 Earth Pressure Cells

Nineteen vibrating wire earth pressure cells 9 inches in diameter and 0.4 inches in thickness were used to measure vertical or lateral earth pressures in the MSE wall test sections. Each pressure cell could measure earth pressures up to 70 psi and measure temperature through a thermistor inside the cell. Among all the pressure cells, four pressure cells were used to measure vertical earth pressures (referred to as vertical pressure cells) while fifteen pressure cells were used to measure lateral earth pressures (referred to as lateral pressure cells). They were calibrated in the lab prior to installation. Four vertical pressure cells were installed in TS2. The vertical pressure cells were placed close to the middle of the section at the bottom of the wall, which were located at about 3.3, 10, 20, and 40 ft behind the wall facing, respectively. The vertical pressure cells were placed horizontally on sand pads with PVC pipes used for the protection of pressure cell cables. Fifteen lateral pressure cells were installed in three MSE wall test sections in total; each wall section was instrumented with five lateral pressure cells along the wall height. Each lateral pressure cell was mounted on a plywood board. The mounted pressure cells were attached on the back of the wall facing and were covered by sand. The locations of the vertical and lateral pressure cells in three MSE wall test sections can be seen in Figure 4.3. Figure 4.6 provides the photographs of the installation of the vertical and lateral pressure cells.

(a) Vertical pressure cell

(b) Lateral pressure cells

Figure 4.6: Vertical and Lateral Pressure Cells Installations

4.5.3 Strain Gauge

The strains of the primary geogrids and secondary geogrids were measured by foil-type strain gages. This type of strain gage had a matrix length of 0.32 inches and a matrix width of 0.17 inches, and could measure a tensile strain up to 3% by a data recorder with 120-ohm resistance. Primary geogrids were instrumented with 120 strain gages, while secondary geogrids were instrumented with 40 strain gages. The locations of strain gages on primary geogrids and secondary geogrids in three test wall sections are shown in Figure 4.7. The installation of strain gages on the geogrids was prepared and completed in the laboratory at the University of Kansas. A geogrid was cut to the specific length based on the design length and the locations for strain gauges were marked along the geogrid. The installation procedures of strain gages on the geogrid mainly included geogrid surface smoothening, surface cleaning, strain gage bonding, protection coating, and cable splicing. The method of strain gage installation is important to the survivability and measurement accuracy of geogrid strains; therefore, the appropriate installation procedure was reviewed, improved, and followed. Five layers of primary geogrids in each MSE wall test section were selected. Each layer of primary geogrid was instrumented with eight strain gages at seven locations: 0.75 (middle of the first aperture), 2.25 (middle of the second aperture), 3.75 (middle of the third aperture), 10, 20, 30, and 50 ft from the first transverse bar. A pair of strain gages was bonded to two sides of geogrid at the location of 0.75 ft from the first transverse bar. Two strain gages were used to eliminate the bending effect of the geogrid. All the strain gages were installed in the middle point of the longitudinal rib between two transverse bars. Five layers of UX1 secondary geogrids and five layers of BX secondary geogrids were selected and instrumented with strain gages in TS1 and TS2, respectively. Each layer of secondary geogrid had four strain gages attached at locations of 0.75, 2.25, and 3.75 ft from the first transverse bar. A pair of strain gages was bonded on two sides of the secondary geogrid at the same location of 0.75 ft from the first transverse bar with the purpose of eliminating the bending effect of the geogrid. The photographs of the installation of primary geogrids and secondary geogrids are provided in Figure 4.7.

(a) Primary uniaxial geogrid

(b) Secondary uniaxial geogrid

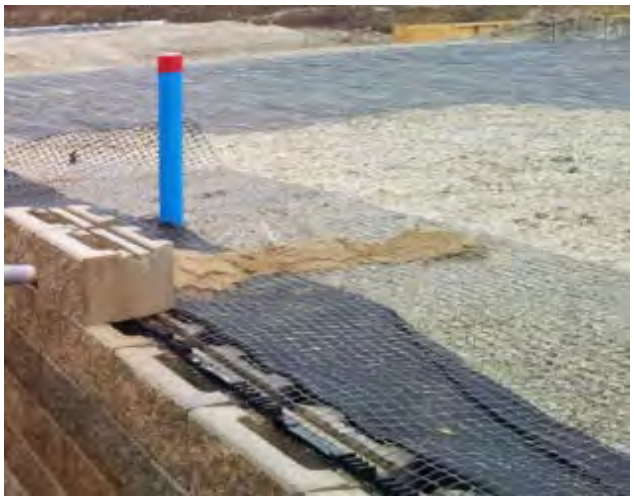

(c) Secondary biaxial geogrid

Figure 4.7: Installation of Geogrids

4.6 Instrumentation Results

4.6.1 Wall Facing Deflections

The profiles of measured wall facing deflections with wall height before and after the construction of the backslope are shown in Figure 4.8. The measured wall facing deflections in the three test wall sections increased with the wall height. The maximum deflections occurred at the top of the wall. As Figure 4.8(a) is compared with Figure 4.8(b), the wall facing deflections increased with the construction of the backslope because additional lateral earth pressure due to the weight of the backslope was applied on the wall facing. In addition, the measured wall facing deflections within the upper part of the walls in TS1 and TS2 were lower than those in TS3 (i.e., the control section), indicating that the inclusion of secondary reinforcement reduced the wall facing deflections.

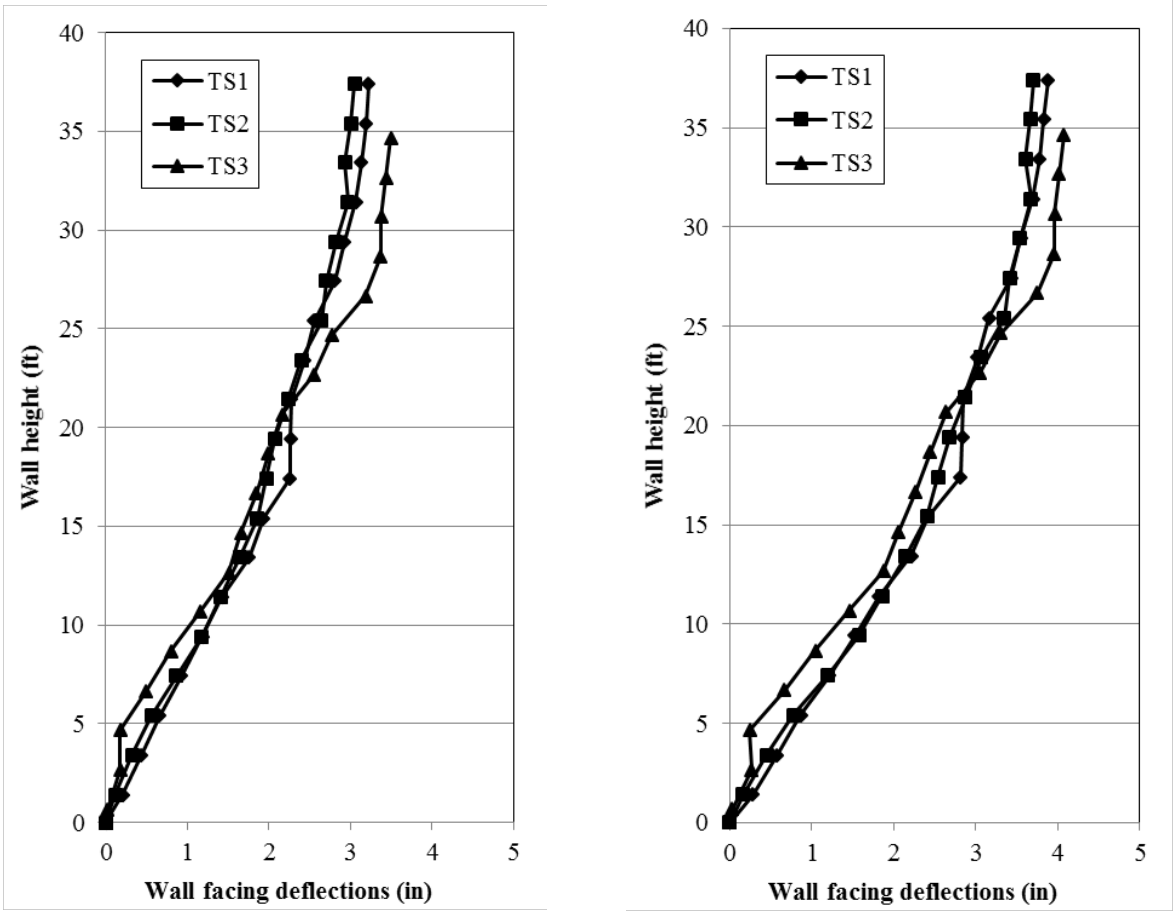

(a) Before the construction of the backslope (b) After the construction of the backslope

Figure 4.8: Profiles of Wall Deflections with the Full Wall Height

Figure 4.8 also shows that at the lower part of the wall, the wall facing deflection in TS3 was smaller than those in TS1 and TS2. This phenomenon can be explained that TS3 had more embedment than TS1 and TS2 during the construction, which means that the passive resistance had more effects on the wall facing deflection of TS3. In order to eliminate the influence of passive resistance, the wall facing deflections at the location of the ground surface in front of the wall were set to be zero and then the profiles of wall facing deflection with free wall height (i.e., the full wall height minus the embedment depth) were obtained and compared among three test wall sections, as illustrated in Figure 4.8. At the lower part of the walls, the wall facing deflections were almost same for the three test wall sections due to close primary reinforcement spacing, while at the upper part of the walls, the inclusion of the secondary reinforcement reduced more wall facing deflections.

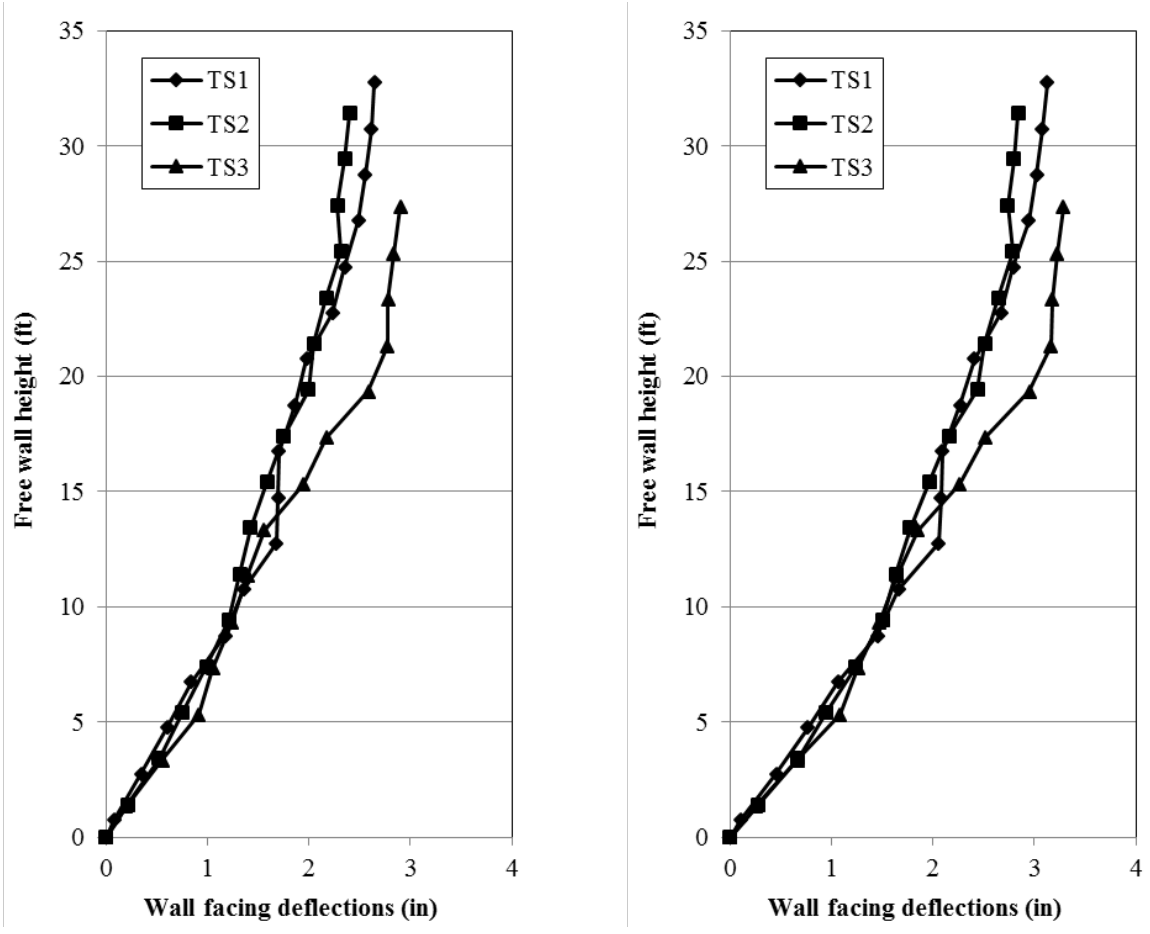

(a) Before the construction of the backslope (b) After the construction of the backslope

Figure 4.9: Profiles of Wall Deflections with the Free Wall Height

Figure 4.10 shows the development of the maximum wall facing deflection with the wall height during construction. The maximum wall facing deflection increased with the increase of the wall height in the three test wall sections. The maximum wall facing deflections were much smaller than 1/75H (H is the wall height), which was an empirical value recommended by Elias and Christopher (1997) to estimate the maximum lateral displacement of wall facing during construction.

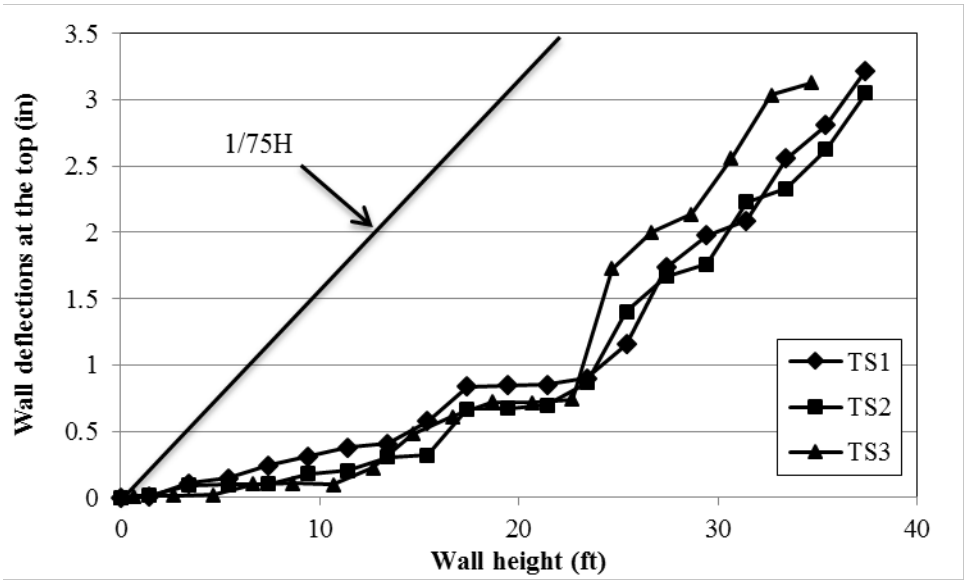

Figure 4.10: Development of the Maximum Wall Facing Deflection with the Wall Height

After the completion of the construction, the monitoring of wall facing deflections of test walls continued monthly until May 2015. Figure 4.11 show the developments of wall facing deflections after construction for three test wall sections. The wall facing deflections increased during the first 4 months after construction and then reached a steady state. The developments of wall facing deflections for three test sections fell in the range of 0.2 and 0.4 inches, which were approximately 0.2 to 0.4% of the wall height.

Similar to Figure 4.8, Figure 4.12 shows that the measured wall facing deflections at the upper part of the wall in TS1 and TS2 were lower than those in TS3 (i.e., the control section), which means that secondary reinforcements reduced the wall facing deflections after construction.

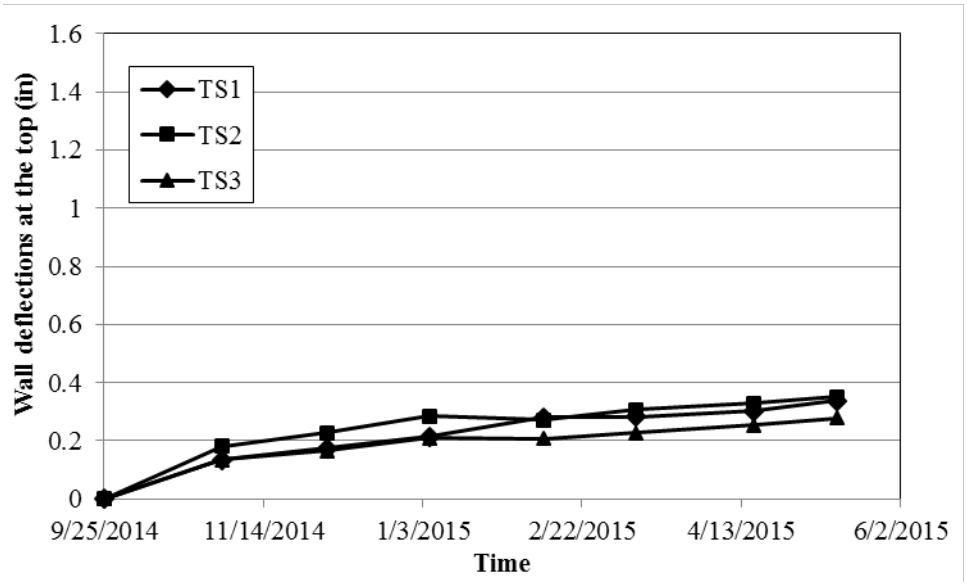

Figure 4.11: Wall Facing Deflections After Construction

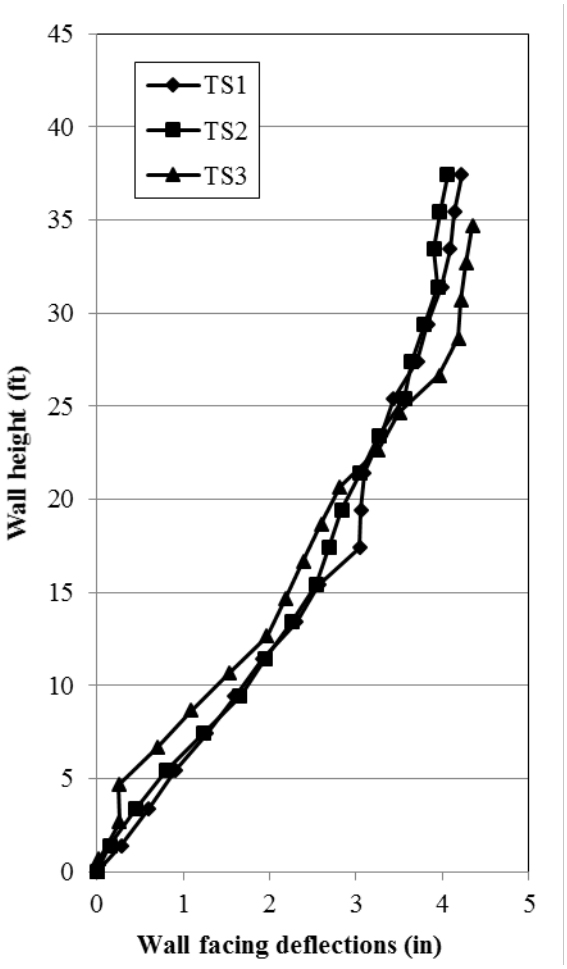

Figure 4.12: Profiles of Wall Deflections with Full Wall Height on May 13, 2015

4.6.2 Vertical Earth Pressures

Figure 4.13(a) presents an increase of the measured vertical earth pressures during construction at different locations in TS2. The overburden stress at the location of 4 was calculated to compare with the corresponding measured vertical earth pressure as shown in Figure 4.13(a). Overall, the calculated overburden stress matched well with the measured vertical earth pressure. In addition, a backslope was constructed on the top of the wall within a short time at the end of the wall construction. The measured vertical earth pressure and calculated overburden stress at the location of 4 captured a rapid increase in the vertical earth pressure induced by the weight of the backslope. However, the measured vertical earth pressure at the location of 2 was unexpectedly low during construction. The result of such a low earth pressure may be explained by a malfunctioned earth pressure cell or deserve a further investigation.

After the construction of the test walls, the vertical earth pressures were still measured every month. Figure 4.13(b) presents the development of the measured vertical earth pressures after the construction of the test wall at different locations in TS2. The calculated vertical earth pressures captured the variation of the measured ones. Both the measured and calculated vertical earth pressures kept stable after the construction of test walls.

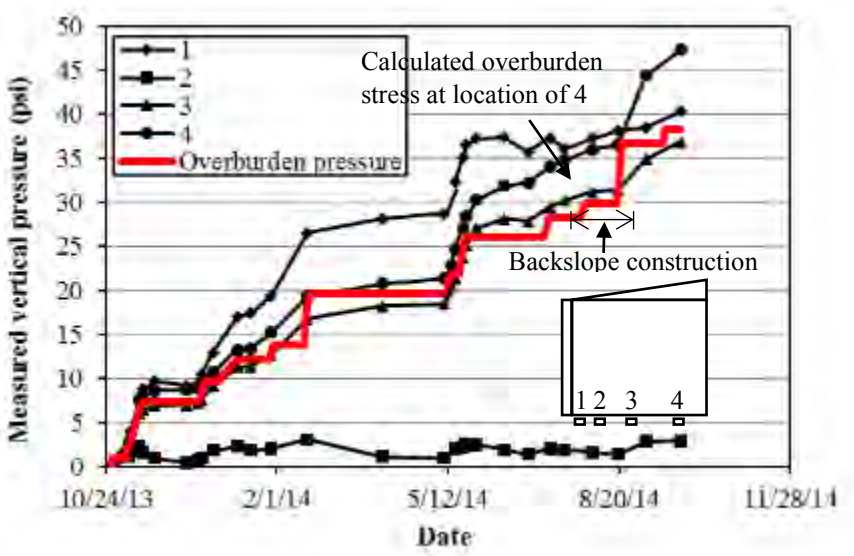

(a) During construction

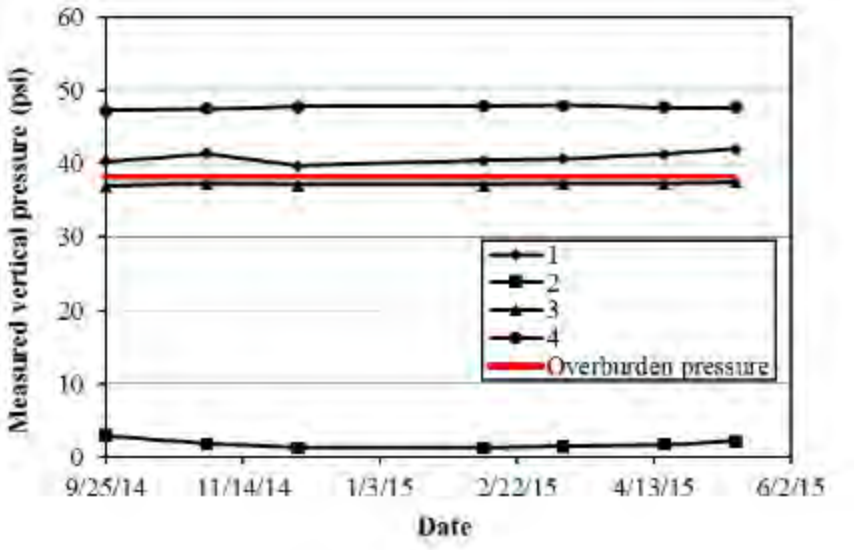

(b) After construction

Figure 4.13: Development of Measured Vertical Earth Pressures

Vertical earth pressures at the bottom of an MSE wall are often not uniform due to external lateral earth pressures from retained soil. The distribution of the vertical earth pressures can be approximated as a trapezoid distribution with the maximum pressure at the toe of the wall and the minimum pressure at the end of reinforcement. The distribution of the measured vertical earth pressures, the calculated overburden stresses, and the trapezoid distribution of the vertical stresses from wall facing before and after the construction of the backslope are presented in

Figure 4.14. Before the construction of the backslope, the measured vertical earth pressures were slightly higher than the calculated overburden stresses and the trapezoidally-distributed stresses. The measured vertical stress close to the wall facing was higher than those away from the wall facing because the lateral earth pressure from the retained soil resulted in potential overturning of the backfill soil towards the toe of the wall and increased the vertical stress close to the wall facing. This distribution is often approximated in a trapezoid shape. However, the distribution of the calculated overburden stresses from the wall facing was uniform because the calculation of the overburden stress did not consider the lateral earth pressure from the retained soil.

After the construction of the backslope, the measured vertical earth pressures increased due to the construction load. In addition, the measured vertical earth pressures were slightly higher than the calculated overburden stresses as well. However, the shape of the distribution of the measured vertical earth pressures after the construction of the backslope changed as compared with that before the construction of the backslope. The measured vertical earth pressures close to the wall facing were lower than those away from the wall facing because the existence of backslope acted as an eccentric load around the toe of the wall in the clockwise direction. This distribution shape was reflected in both the calculated overburden stresses and the trapezoidally-distributed stresses. In addition, the calculated overburden stresses were lower than the calculated trapezoidally-distributed stresses at the locations close to the wall facing, while the calculated overburden stresses became higher than the calculated trapezoidally-distributed stresses at the locations away from the wall facing. This phenomenon is attributed to the existence of the backslope as an eccentric load.

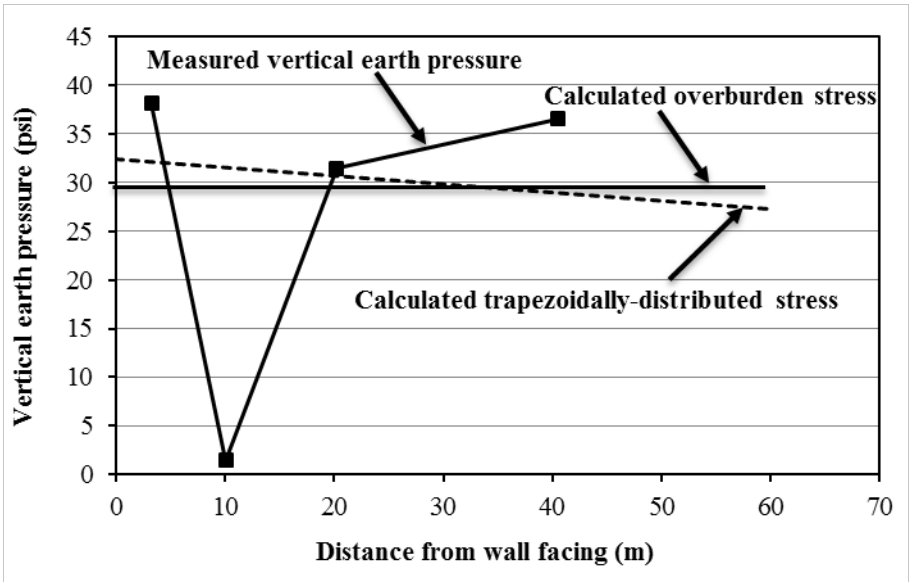

(a) Before the construction of the backslope

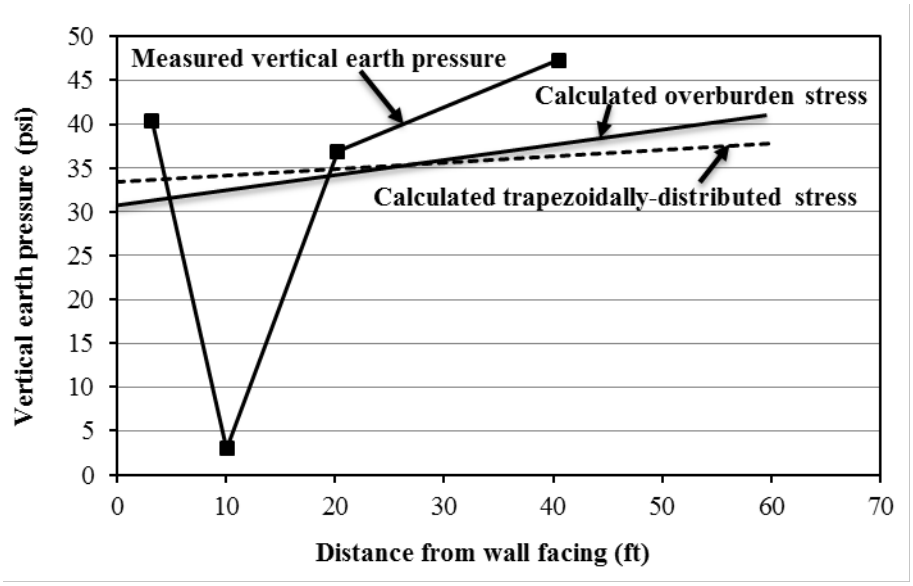

(b) After the construction of the backslope

Figure 4.14: Distributions of Measured and Calculated Vertical Earth Pressures from Wall Facing

4.6.3 Lateral Earth Pressures

Figure 4.15 show the development of the lateral earth pressures for all three test sections. The lateral earth pressures in each test section gradually increased during the construction and remained constant after the construction.

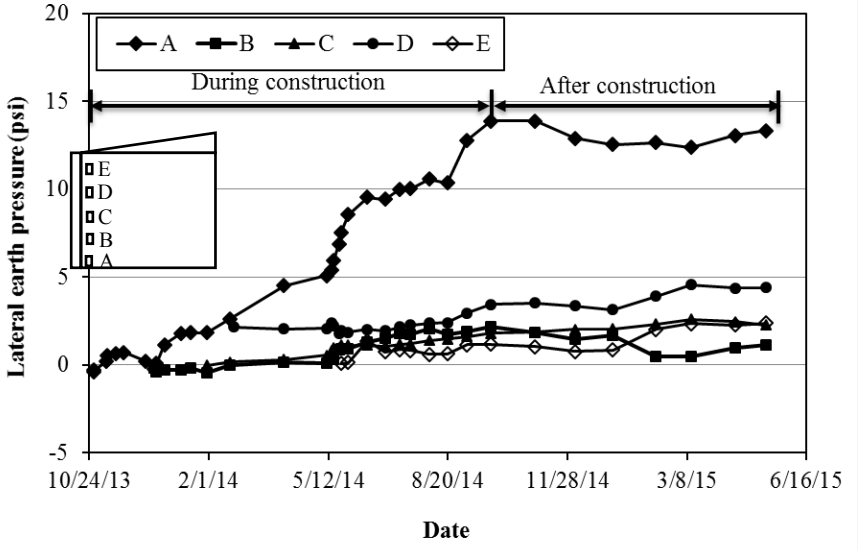

(a) TS1

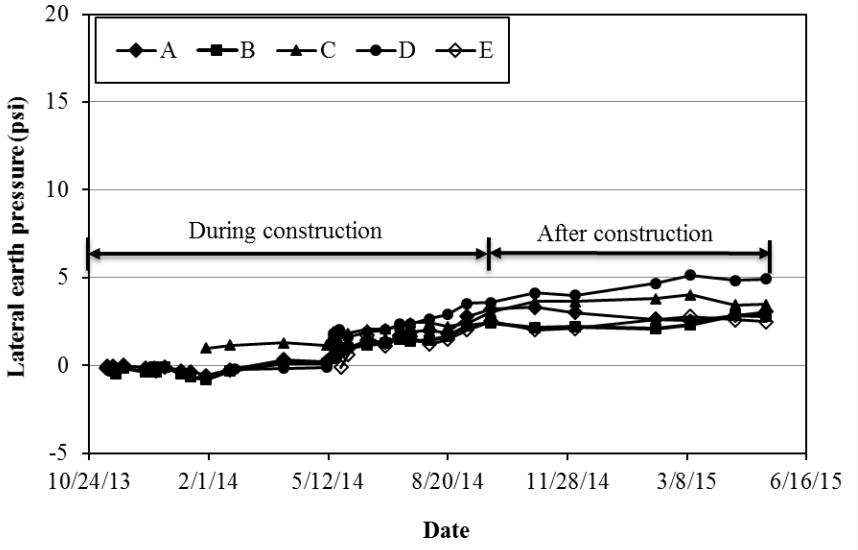

(b) TS2

Figure 4.15: Development of Measured Lateral Earth Pressures

(c) TS3

Figure 4.15: Development of Measured Lateral Earth Pressures (Continued)

The profiles of the measured lateral earth pressures for the three test wall sections at the end of the construction are presented in Figure 4.16. For a comparison, the at-rest earth pressures were calculated. Additionally, the active earth pressures were calculated at two different friction angles using the AASHTO (2007) method based on Rankine's earth pressure theory. The adopted Rankine's theory in the AASHTO method considered the backslope on the top of the wall and the coefficient of active earth pressure was calculated by Equation 4.1:

$$K_a = \cos\beta\left[\frac{\cos\beta - \sqrt{\cos^2\beta - \cos^2\phi}}{\cos\beta + \sqrt{\cos^2\beta - \cos^2\phi}}\right] \qquad \textbf{Equation 4.1}$$

Where:

ϕ is the design friction angle of the aggregate, and

β is the angle of the backslope.

The calculated active earth pressures using the design friction angles of 34° overall were higher than the measured earth pressures. This result indicates that the friction angle of 34° used in the calculation of the active earth pressure was too conservative.

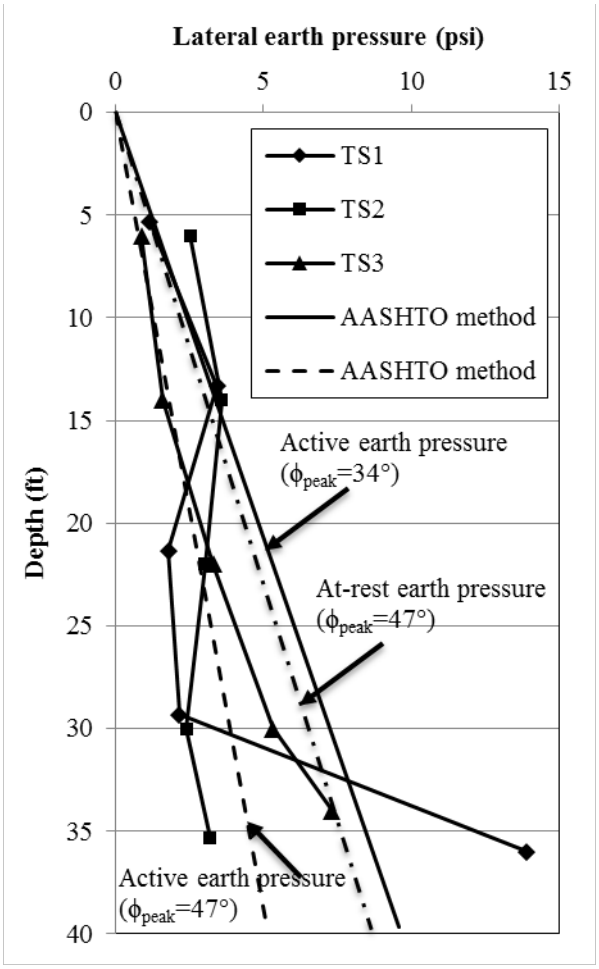

Figure 4.16: Profiles of Measured Lateral Earth Pressures

In TS3 (i.e., the control section), the measured lateral earth pressures increased approximately linearly with depth, which fell between the calculated active earth pressures and the at-rest earth pressures using the actual friction angle of 47° measured from the triaxial shear tests. The measured earth pressures within the lower part of the wall were close to the at-rest earth pressure because the existence of the embedment limited wall deflection and constrained the mobilization of the backfill soil at the bottom of the wall. However, the measured earth pressures within the upper part of the wall were close to the active earth pressure because the wall deflection was sufficient to allow the fill to be in an active state.

As compared with the linear distribution of the measured lateral earth pressures in TS3, the distribution of the measured lateral earth pressures in TS1 and TS2 (i.e., the test wall sections reinforced by secondary geogrids) were approximately uniform. The active earth pressures

within the upper part of the wall are close to the at-rest earth pressures because the existence of secondary reinforcement reduced the wall facing deflection and limited the mobilization of the reinforcement and backfill within the upper part of the wall. Moreover, the measured lateral earth pressure at the depth of 37.1 ft in TS1 was unreasonable because its magnitude was far higher than other measured values. A further analysis is needed to examine the validity of this measured value.

Figure 4.17 shows that the distribution of the coefficient of lateral earth pressure normalized by the coefficient of active earth pressure calculated based on Rankine's earth pressure theory. In addition, the distributions of the coefficient of lateral earth pressure in MSE walls reinforced by other reinforcements are presented (Christopher et al., 1989). The coefficient of lateral earth pressure was back calculated from the measured earth pressure and the calculated overburden stress. The ratios of the coefficient of lateral earth pressure to that of active earth pressure in the control section (i.e., TS3) were approximately uniform and close to 1.0. This result was consistent with those presented by Christopher et al. for geosynthetics as shown in Figure 4.17. However, the distributions of coefficient of lateral earth pressure in the test sections reinforced by secondary reinforcements were different from that in the control section. The coefficients of lateral earth pressure in TS1 and TS2 decreased with depth when the depth was less than 20 ft. Furthermore, the coefficients were greater than that in TS3 and approached to the ones in MSE walls reinforced by steel reinforcements. This phenomenon can be explained that the inclusion of the secondary reinforcement reduced wall facing deflection as steel reinforcement, resulting in a larger ratio of the coefficient of lateral earth pressure to that of active earth pressure.

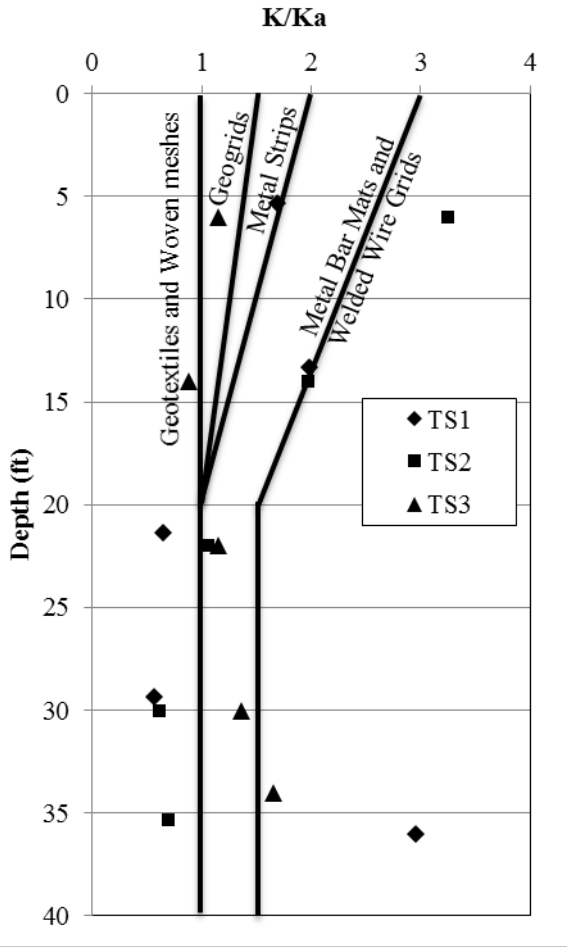

Figure 4.17: Distribution of Coefficient Ratio of Lateral Earth Pressure with Depth

4.6.4 Global Strains of Geogrids

Figure 4.18 shows the global strains of primary and secondary geogrids at five instrumented layers in the three test wall sections at the end of the construction. The global strains as shown in Figure 4.18 were calculated by the measured local strains multiplying the CFs between local strains and global strains determined in the laboratory as discussed earlier. Figure 4.18(a) shows that for each instrumented layer, the strains of primary geogrids increased along the geogrids to reach the maximum and then reduced to be zero at a distance away from the wall facing. This distance represented the length of interaction between geogrid and soil. Leshchinsky et al. (2014) found that this interaction distance became larger with an increase of wall height. A solid line was drawn as a profile identifying the locations of these interaction distances. The measured strains well captured this trend. In addition, the measured strains of

geogrids in all three test wall sections were all far smaller than the design strains calculated by the design stresses.

Figure 4.18(b) presents the global strains of secondary geogrids in TS1 and TS2 at the end of the construction. It is shown that the secondary geogrids carried tensile loads so that the tensile loads in the primary geogrids were reduced.

Figure 4.18 also shows some negative strains in the geogrids. These negative strains might be caused by the bending moments on the geogrids at the instrumented locations. The negative strains might also result from the compression of the geogrids induced by the lateral earth pressure from the retained soil. Additionally, the measured global strains of the geogrids at the connections were very low, indicating that the connection forces were low too. Initial readings of the strains of the geogrids were taken after the one lift of aggregate was placed and compacted. The strains of geogrids due to displacement of modular blocks during the compaction of the backfill soil were not measured. Moreover, Leshchinsky et al. (2014) found low connection forces using the limit equilibrium method to calculate the tension force in the reinforcement in an MSE wall.

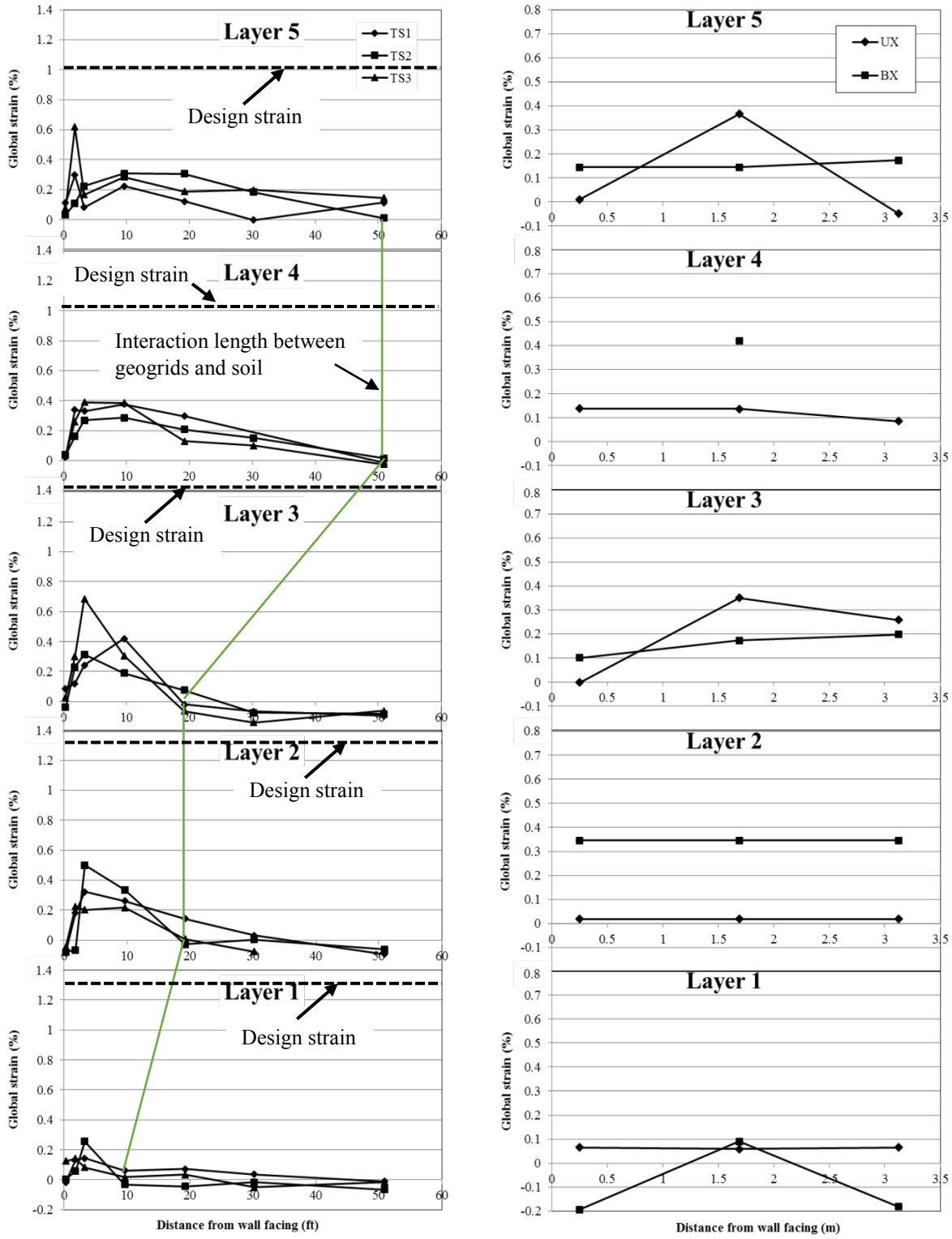

(a) Primary geogrids (b) Secondary geogrids

Figure 4.18: Global Strains of Geogrids in the MSE Wall Test Sections

Figure 4.19 presents the profile of the maximum strains with depth for all three test wall sections. The maximum strains for all three test wall sections occurred at the locations close to the wall facing within the reinforced backfill zone. The maximum strains ranged from 0.15 to 0.43%, 0.26 to 0.5%, and 0.14 to 0.69%, for TS1, TS2, and TS3, respectively. Figure 4.19 also shows that the maximum strains of the primary geogrids at the instrumented layers above the embedment (Layers 3, 4, and 5) in TS3 were larger than those in TS1 and TS2. This result can be explained that the secondary reinforcements in TS1 and TS2 carried a portion of the tension forces from the lateral earth pressures and reduced the maximum tension forces in the primary geogrids.

However, the maximum strains of the primary geogrids at the first two instrumented layers (i.e., Layers 1 and 2) in TS3 were smaller than those in TS1 and TS2. This result can be attributed to the influence of the embedment. TS3 had more embedment than TS1 and TS2 after the first construction of embedment (i.e., the construction on November 22, 2013). The three test wall sections had the same embedment after the second construction of embedment (i.e., the construction on March 24, 2014). The two embedment lines at the two times are illustrated in Figure 4.2. As compared with TS3, the embedment in TS1 and TS2 had less influence on the reduction of the strains of the primary geogrids at first two layers.

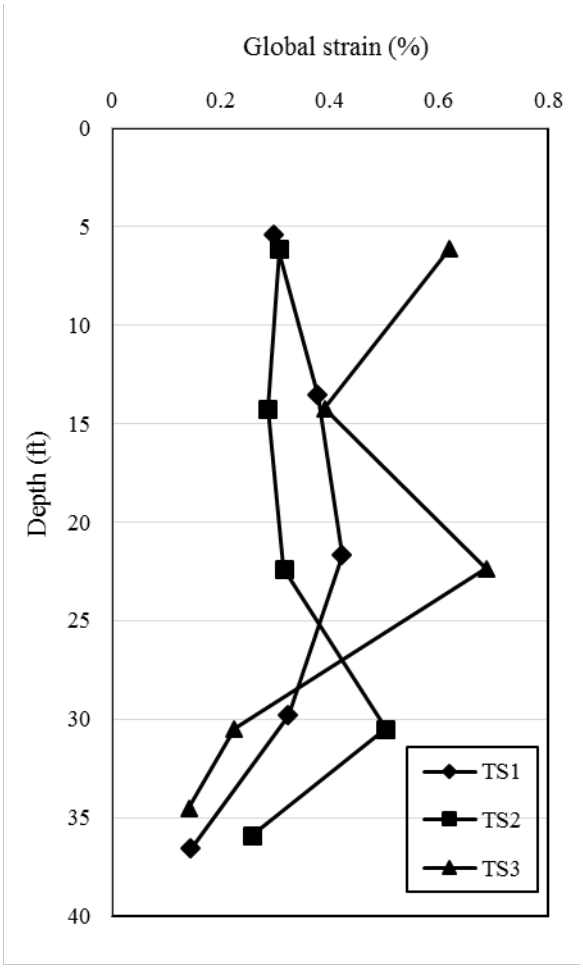

Figure 4.19: Profiles of Maximum Global Strains of Primary Geogrids

Chapter 5: Proposed Design Guidelines

5.1 Introduction

Based on field measurements and data analysis in previous chapters, design guidelines are proposed in this chapter to design an MSE wall with secondary reinforcements. Since secondary reinforcements are placed close to wall facing, they do not have any effect on external stability of MSE walls. For the external stability design, therefore, an MSE wall with secondary reinforcements should follow the same design guideline for an MSE wall without secondary reinforcements as presented in AASHTO (2012). For the internal stability, however, secondary reinforcements can have some effects. Design guidelines are proposed for internal stability analysis of MSE walls with secondary reinforcements based on the field performance of the test walls with secondary reinforcements in this study. These design guidelines are only applicable for internal stability design of MSE walls with secondary reinforcements under static loading.

5.2 General Design Procedure

Similar to the MSE walls without secondary reinforcements, there are two internal failure modes that may happen in the MSE walls with secondary reinforcements: (1) the failure due to excessive elongation or rupture of primary and secondary reinforcements; and (2) the failure due to insufficient pullout capacities of primary and secondary reinforcements. In order to prevent these two failure modes, the maximum tensile forces, the pullout capacities, and the tensile strengths of primary and secondary reinforcements should be determined.

A step-by-step internal stability design for an MSE wall with secondary reinforcements is given in Table 5.1.

Table 5.1: Design Procedure for an MSE Wall with Secondary Reinforcements

Step	Design Procedure
1	Select the geosynthetic type for primary and secondary reinforcements.
2	Select a spacing compatible with the facing for primary and secondary reinforcements.
3	Calculate the lateral earth pressure at each reinforcement level for primary and secondary reinforcements.
4	Calculate the maximum tensile force at each reinforcement level for primary and secondary reinforcements.
5	Calculate the maximum tensile force at the connection to the facing for primary and secondary reinforcements.
6	Calculate the allowable stress for primary and secondary reinforcements.
7	Calculate the pullout capacity at each reinforcement level for primary and secondary reinforcements.

Note: This design procedure is modified from AASHTO (2012).

5.3 Lateral Earth Pressure Distribution

According to the measurements of the test walls, MSE walls reinforced with secondary geogrids have a different distribution of lateral earth pressures from MSE walls without secondary reinforcements. To determine the lateral earth pressure in an MSE wall with secondary reinforcements, the following assumptions are made:

1. Lateral earth pressure is trapezoidally distributed as shown in Figure 4.16, which has a linearly distributed pressure from the top of wall to a turning point and then has uniformly distributed pressure to the bottom of wall;
2. The linearly-distributed lateral earth pressure is under the at-rest state;
3. The total force from the trapezoidally-distributed lateral earth pressure is equal to the total force from the linearly-distributed lateral earth pressure based on the Rankine or Coulomb active earth pressure theory.

Based on these assumptions, Equation 5.1 is obtained:

$$0.5K_a\gamma H^2 = 0.5K_0\gamma H_1^{\ 2} + K_0\gamma H_1 H_2 \qquad \textbf{Equation 5.1}$$

Where:

H is the height of the wall;

H_1 is the height of the linearly-distributed lateral earth pressure, which is from the top of the wall to the turning point;

$H_2 = H - H_1$ is the height of uniformly-distributed lateral earth pressure, which is from the turning point to the bottom of wall;

γ is the unit weight of backfill soil;

K_a is the coefficient of active earth pressure using the Rankine or Coulomb theory; and

K_0 is the coefficient of earth pressure at rest.

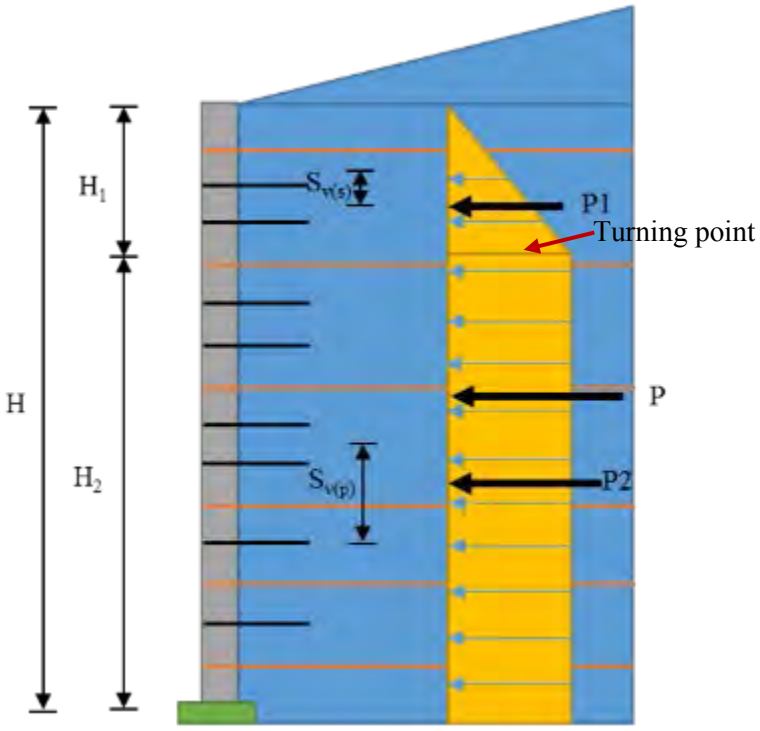

Figure 5.1: Proposed Distribution of Lateral Earth Pressure

H_1 can be solved by Equation 5.1, then the factored lateral earth pressure can be expressed by Equation 5.2:

$$\sigma_H = \begin{cases} \gamma_p\left(K_0\gamma h + \Delta\sigma_H\right) & 0 \le h < H_1 \\ \gamma_p\left(K_0\gamma H_1 + \Delta\sigma_H\right) & H_1 \le h \le H \end{cases} \qquad \textbf{Equation 5.2}$$

Where:

γ_p is the load factor for vertical earth pressure that is included in Table 3.4.1-2 in AASHTO (2012), and

$\Delta\sigma_H$ is the horizontal stress at the reinforcement level resulting from an applicable concentrated horizontal surcharge load as specified in Article 11.10.10.1 in AASHTO (2012).

5.4 Maximum Tensile Forces in Primary and Secondary Reinforcements

The general design philosophy is that (1) primary reinforcements carry the maximum tensile forces at the Rankine or Coulomb failure plane for globally internal stability, and (2) secondary reinforcements carry the forces behind the wall facing for locally internal stability. Below are the procedures to calculate the maximum tensile forces in primary and secondary reinforcements:

1. For primary reinforcements, the factored maximum tensile force $T_{max(p)}$ per unit width at each reinforcement layer can be calculated by Equation 5.3:

$$T_{max(p)} = \frac{\sigma_H \cdot S_{v(p)}}{R_c} \qquad \textbf{Equation 5.3}$$

Where:

σ_H is the average factored lateral earth pressure within the contributory vertical spacing

$S_{v(p)}$ is the contributory vertical spacing of the primary reinforcements

R_c is the coverage ratio of primary reinforcements

2. For secondary reinforcements, the factored maximum tensile force $T_{max(s)}$ per unit width at each reinforcement layer can be calculated by Equation 5.4:

$$T_{max(s)} = \frac{\sigma_H \cdot S_{v(s)}}{R_c} \quad \textbf{Equation 5.4}$$

Where:

σ_H is the average factored lateral earth pressure within the contributory vertical spacing

$S_{v(s)}$ is the contributory vertical spacing of secondary reinforcements

R_c is the coverage ratio of secondary reinforcements

5.5 Maximum Tensile Force at the Connection

The maximum tensile force at the connection for primary and secondary reinforcements can be assumed to be $T_{max(s)}$, which is much lower than the maximum tensile force in the primary reinforcement.

5.6 Allowable Tensile Strengths for Primary and Secondary Reinforcements

Allowable tensile strengths for primary and secondary reinforcements can be calculated by the following procedure:

1. For each primary reinforcement, the factored allowable tensile strength $T_{a(p)}$ is calculated using Equation 5.5:

$$T_{a(p)} = \phi \cdot \frac{T_{ult(p)}}{RF_p} \geq T_{max(p)} \quad \textbf{Equation 5.5}$$

Where:

$T_{ult(p)}$ is the ultimate forces of primary reinforcement

RF_p is the reduction factor of primary reinforcement

ϕ is the resistance factor for reinforcement tension in Table 11.5.7-1 in AASHTO (2012)

2. For each secondary reinforcements, the factored allowable tensile strength $T_{a(s)}$ is calculated using Equation 5.6:

$$T_{a(s)} = \varphi \cdot \frac{T_{ult(s)}}{RF_s} \geq T_{\max(s)} \qquad \textbf{Equation 5.6}$$

Where:

$T_{ult(s)}$ is the ultimate force of secondary reinforcement

RF_s is the reduction factor of secondary reinforcement

ϕ is the resistance factor for reinforcement tension in Table 11.5.7-1 in AASHTO (2012)

5.7 Pullout Capacities for Primary and Secondary Reinforcements

Pullout capacities for primary and secondary reinforcements can be calculated in the following procedure:

1. For primary reinforcements, the factored pullout capacity $T_{po(p)}$ is calculated using Equation 5.7:

$$T_{po(p)} = \phi \cdot F^* \cdot \gamma \cdot Z_p \cdot L_e \cdot C \cdot R_c \cdot \alpha \geq T_{\max(p)} \qquad \textbf{Equation 5.7}$$

Where:

ϕ is the resistance factor for reinforcement pullout from Table 11.5.7-1 in AASHTO (2012)

F^* is the pullout resistance factor

$\gamma \cdot Z_p$ is the overburden pressure above the primary reinforcement, including distributed dead load surcharges but neglecting traffic loads

L_e is the length of embedment in the resisting zone

C is equal to 2

R_c is the coverage ratio of primary reinforcement

α is the scale correction factor

The calculation of the length embedded in the resisting zone can use Equation 5.8:

$$L_e = L - L_a \qquad \textbf{Equation 5.8}$$

Where:

L is the total length of primary reinforcement, and

$$L_a = (H - Z_p)\tan\left(45° - \frac{\phi}{2}\right)$$

H is the height of wall, Z_p is the depth of primary reinforcement

ϕ is friction angle of backfill soil

2. For secondary reinforcements, the factored pullout capacity $T_{po(s)}$ is calculated using Equation 5.9:

$$T_{po(s)} = \phi \cdot F^* \cdot \gamma \cdot Z_s \cdot L_{e(s)} \cdot C \cdot R_c \cdot \alpha \geq T_{\max(s)} \qquad \textbf{Equation 5.9}$$

Where:

ϕ is the resistance factor for reinforcement pullout from Table 11.5.7-1 in AASHTO (2012)

F^* is the pullout resistance factor

$\gamma \cdot Z_s$ is the overburden pressure above the secondary reinforcement, including distributed dead load surcharges but neglecting traffic loads

$L_{e(s)}$ is the length of secondary reinforcement

C is equal to 2

R_c is coverage ratio of secondary reinforcement

α is the scale correction factor

5.8 Design Example

To illustrate the proposed guideline for the internal stability design of an MSE wall with secondary reinforcements, a design example is provided in this section. TS1 in the field test is selected as the example. A step-by-step calculation is provided as follows:

1. Selection of reinforcements

Four types of uniaxial geogrids and one type of uniaxial geogrid were selected as primary and secondary reinforcements for TS1, respectively. The properties of these geogrids can be found in Table 3.1.

2. Selection of reinforcement spacing

The primary geogrids were vertically spaced with two distances, which are 16 inches and 24 inches. The secondary geogrids were vertically spaced every 8 inches, except the level of primary geogrids. More details regarding the spacing of geogrids in TS1 can be found in Figure 4.3(a).

3. Calculation of lateral earth pressure

Wall height H = 39 ft
Unit weight γ = 114.8 pcf
Friction angle φ = 47°
Batter angle ω = 0.45°
Backslope angle β = 14°

Since the batter angle of the wall (0.45°) is less than 10°, the Rankine theory is used to calculate the coefficient of active earth pressure:

$$K_a = \cos\beta\left[\frac{\cos\beta - \sqrt{\cos^2\beta - \cos^2\varphi}}{\cos\beta + \sqrt{\cos^2\beta - \cos^2\varphi}}\right] = \cos 14°\left[\frac{\cos 14° - \sqrt{\cos^2 14° - \cos^2 47°}}{\cos 14° + \sqrt{\cos^2 14° - \cos^2 47°}}\right] = 0.163$$

The coefficient of earth pressure at rest is:

$$K_0 = 1 - \sin\varphi = 1 - \sin 47° = 0.269$$

Substitute all values of the variables in Equation (5.1) and solve H_1 and H_2:

$$0.5K_a\gamma H^2 = 0.5K_0\gamma H_1^{\,2} + K_0\gamma H_1\left(H - H_1\right)$$

$$0.5\times 0.163\times 115.2\times 39^2 = 0.5\times 0.269\times 115.2\times H_1^{\,2} + 0.269\times 115.2\times H_1(39 - H_1)$$

$$H_1 = 14.4 \text{ ft}$$

$$H_2 = 39 - 14.4 = 24.6 \text{ ft}$$

The factored lateral earth pressure is:

$$\sigma_H = \begin{cases} 1.3\times 30.9h & 0 \le h \le 14.4 \\ 1.3\times 444.7 & h \ge 14.4 \end{cases} \text{ psf}$$

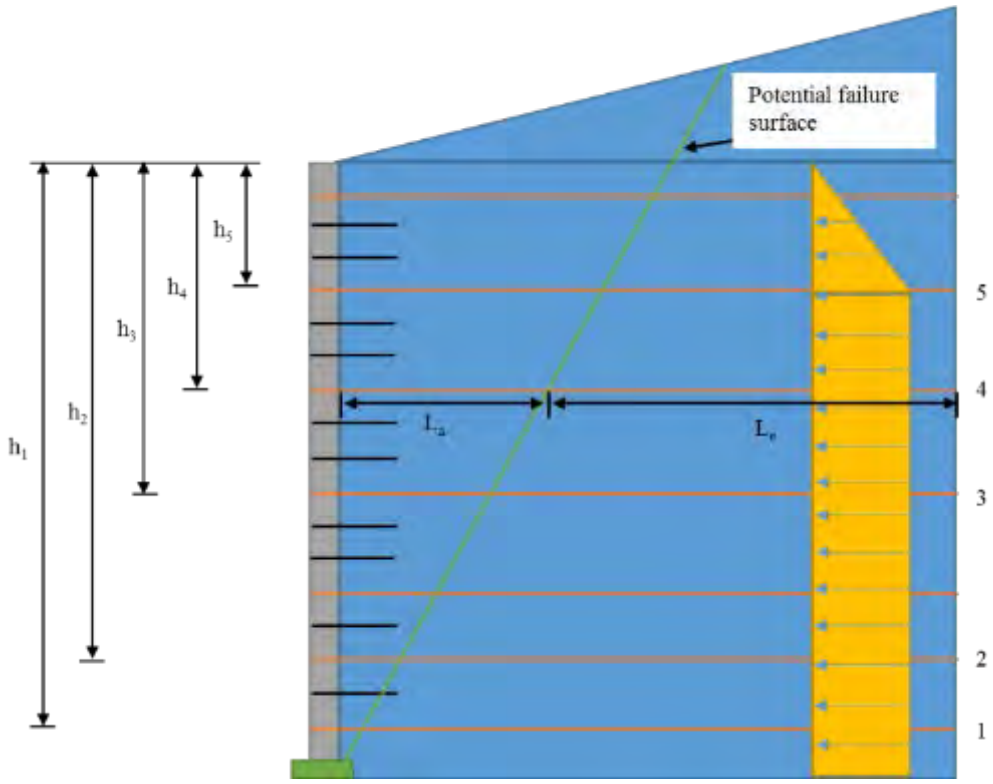

Figure 5.2: Distribution of Lateral Earth Pressure (Not to Scale)

4. Calculation of maximum tensile force

The instrumented primary and secondary geogrids are selected to calculate the maximum tensile forces. The coverage ratios of primary and secondary geogrids are 1.0. The depths of each instrumented primary geogrid are:

$h_1 = 37$ ft; $h_2 = 30.3$ ft; $h_3 = 22.3$ ft; $h_4 = 14.3$ ft; $h_5 = 6.3$ ft

The corresponding factored average lateral earth pressures within the contributory spacing at all instrumented primary geogrids are:

$$\sigma_{h1} = 578.1 \text{ psf};\ \sigma_{h2} = 578.1 \text{ psf};\ \sigma_{h3} = 578.1 \text{ psf};\ \sigma_{h4} = 578.1 \text{ psf};\ \sigma_{h5} = 558.4 \text{ psf}$$

The corresponding contributory vertical spacing for all instrumented primary geogrids is:

$$S_{v(p1)} = 1.33 \text{ ft};\ S_{v(p2)} = 1.33 \text{ ft};\ S_{v(p3)} = 2 \text{ ft};\ S_{v(p4)} = 2 \text{ ft};\ S_{v(p5)} = 2 \text{ ft}$$

The factored maximum tensile forces of all instrumented primary geogrids are:

$$T_{\max(p1)} = \frac{\sigma_{h1} \cdot S_{v(p1)}}{R_c} = \frac{578.1 \times 1.33}{1} = 768.9 \text{ lbs/ft}$$

$$T_{\max(p2)} = \frac{578.1 \times 1.33}{1} = 768.9 \text{ lbs/ft}$$

$$T_{\max(p3)} = \frac{578.1 \times 2}{1} = 1156.2 \text{ lbs/ft}$$

$$T_{\max(p4)} = \frac{578.1 \times 2}{1} = 1156.2 \text{ lbs/ft}$$

$$T_{\max(p5)} = \frac{558.4 \times 2}{1} = 1116.8 \text{ lbs/ft}$$

Similar to the primary geogrids, the factored maximum tensile forces of all instrumented secondary geogrids are:

$$T_{\max(s1)} = \frac{578.1 \times 0.67}{1} = 387.3\,\text{lbs/ft}$$

$$T_{\max(s2)} = \frac{578.1 \times 0.67}{1} = 387.3\,\text{lbs/ft}$$

$$T_{\max(s3)} = \frac{578.1 \times 0.67}{1} = 387.3\,\text{lbs/ft}$$

$$T_{\max(s4)} = \frac{578.1 \times 0.67}{1} = 387.3\,\text{lbs/ft}$$

$$T_{\max(s5)} = \frac{534.3 \times 0.67}{1} = 358.0\,\text{lbs/ft}$$

5. Calculation of allowable strength

For primary geogrids, the resistance factor is taken to be 0.9 according to Table 11.5.7-1 in AASHTO (2012) and the factored allowable tensile strengths are calculated as follows:

$$T_{a(p1)} = \phi \cdot \frac{T_{ult(p)}}{RF_p} = 0.9 \times \frac{9870}{1.05 \times 2.6 \times 1.0} = 3254\ \text{lbs/ft} > T_{\max(p1)} = 768.9\,\text{lbs/ft};$$

$$T_{a(p2)} = 2574\ \text{lbs/ft} > T_{\max(p2)} = 768.9\,\text{lbs/ft};$$

$$T_{a(p3)} = 3258\,\text{lbs/ft} > T_{\max(p3)} = 1156.2\,\text{lbs/ft};$$

$$T_{a(p4)} = 2574\,\text{lbs/ft} > T_{\max(p4)} = 1156.2\,\text{lbs/ft};$$

$$T_{a(p5)} = 1305\,\text{lbs/ft} > T_{\max(p5)} = 1116.8\,\text{lbs/ft}.$$

For secondary geogrids, the factored allowable tensile strength is calculated as follows:

$$T_{a(s)} = 1450\ \text{lbs/ft}.$$

The factored allowable tensile strength is higher than the factored maximum tensile forces.

6. Calculation of pullout capacity

$$F^* = 0.8 \cdot \tan(\varphi) = 0.8 \times \tan(47°) = 0.86$$

$$C = 2$$

$$R_c = 1$$

$$\alpha = 0.8$$

For instrumented primary geogrids, the lengths of primary geogrids embedded in the resisting zone are:

$$L_{e(p1)} = L - L_a = L - (H - Z)\tan(45° - \frac{\varphi}{2})$$

$$= 62 - (39 - 37)\tan(45° - \frac{47°}{2}) = 61.2 \quad \text{ft}$$

$$L_{e(p2)} = 58.6\,\text{ft}$$

$$L_{e(p3)} = 55.4\,\text{ft}$$

$$L_{e(p4)} = 52.3\,\text{ft}$$

$$L_{e(p5)} = 49.1\,\text{ft}$$

The overburden stresses above primary geogrids are:

$$\gamma \cdot Z_{p1} = 114.8 \times 37 + 740 = 4987.6 \text{ psf}$$

$$\gamma \cdot Z_{p2} = 4218.4 \text{ psf}$$

$$\gamma \cdot Z_{p3} = 3300 \text{ psf}$$

$$\gamma \cdot Z_{p4} = 2381.6 \text{ psf}$$

$$\gamma \cdot Z_{p5} = 1463.2 \text{ psf}$$

The factored pullout capacities for the instrumented primary geogrids are:

$$T_{po(p1)} = \phi \cdot F^* \cdot \gamma \cdot Z_{p1} \cdot L_{e(p1)} \cdot C \cdot R_c \cdot \alpha \text{ lb/ft}$$

$$= 0.9 \times 0.86 \times 4987.6 \times 61.2 \times 2 \times 1 \times 0.8 = 377160 > T_{\max(p1)} = 768.9 \text{ lbs/ft};$$

$$T_{po(p2)} = 305243 \text{ lbs/ft} > T_{\max(p2)} = 768.9 \text{ lbs/ft};$$

$$T_{po(p3)} = 225941 \text{ lbs/ft} > T_{\max(p3)} = 1156.2 \text{ lbs/ft};$$

$$T_{po(p4)} = 153790 \text{ lbs/ft} > T_{\max(p4)} = 1156.2 \text{ lbs/ft};$$

$$T_{po(p5)} = 88790 \text{ lbs/ft} > T_{\max(p5)} = 1116.8 \text{ lbs/ft}.$$

The above factored pullout capacities are much greater than the factored maximum tensile forces; therefore, the design for pullout is overly conservative.

For instrumented secondary geogrids, the lengths of secondary geogrids embedded in the resisting zone (i.e., behind the facing) are:

$$L_{e(s)} = L = 4.5 \text{ ft}$$

The overburden stresses of secondary geogrids are:

$$\gamma \cdot Z_{s1} = 114.8 \times (37 - 0.67) + 740 = 4911 \text{ psf}$$

$$\gamma \cdot Z_{s2} = 4142 \text{ psf}$$

$$\gamma \cdot Z_{s3} = 3224 \text{ psf}$$

$$\gamma \cdot Z_{s4} = 2305 \text{ psf}$$

$$\gamma \cdot Z_{s5} = 1387 \text{ psf}$$

The factored pullout capacities for the instrumented secondary geogrids are:

$$T_{po(s1)} = \varphi \cdot F^{*} \cdot \gamma \cdot Z_{s1} \cdot L_{es} \cdot C \cdot R_{c} \cdot \alpha = 0.9 \times 0.86 \times 4911 \times 4.5 \times 2 \times 1 \times 0.8 = 27301 \text{ lbs/ft}$$

$$T_{po(s2)} = 25584 \text{ lbs/ft}$$

$$T_{po(s3)} = 19911 \text{ lbs/ft}$$

$$T_{po(s4)} = 14238 \text{ lbs/ft}$$

$$T_{po(s5)} = 8565 \text{ lbs/ft}$$

The factored pullout capacities for secondary geogrids are higher than the corresponding factored maximum tensile forces.

7. Comparison between the calculated and measured maximum tensile forces of geogrids

Tables 5.2 and 5.3 summarize the calculated and measured maximum tensile forces of the instrumented primary geogrids and secondary geogrids, respectively. All the calculated maximum tensile forces are mostly 2 times higher than the corresponding measured maximum tensile forces.

Table 5.2: Calculated versus Measured Maximum Tensile Forces of Instrumented Primary Geogrids

Number	Depth (ft)	Calculated maximum tensile force T_{cal} (lbs/ft)	Measured maximum tensile force T_{mea} (lbs/ft)	T_{cal}/T_{mea}
1	37	591.5	125.4	4.7
2	30.3	591.5	248.4	2.4
3	22.3	889.4	364.2	2.4
4	14.3	889.4	289.9	3.1
5	6.3	859.0	121.7	7.1

Table 5.3 Calculated versus Measured Maximum Tensile Forces of Instrumented Secondary Geogrids

Number	Depth (ft)	Calculated maximum tensile force T_{cal} (lbs/ft)	Measured maximum tensile force T_{mea} (lbs/ft)	T_{cal}/T_{mea}
1	36.3	297.9	29.5	10.1
2	29.6	297.9	150.3	2.0
3	21.6	297.9	157.3	1.9
4	13.6	297.9	52.6	5.7
5	5.6	275.4	35.0	7.9

Chapter 6: Summary and Conclusions

In this study, three mechanically stabilized earth (MSE) wall test sections, were instrumented and monitored during the construction with earth pressure cells, inclinometer casings, and strain gauges. The three test sections included one test section (TS1) reinforced with primary and secondary uniaxial geogrids, one test section (TS2) reinforced with primary uniaxial geogrids and secondary biaxial geogrids, and one test section (TS3) reinforced with primary geogrids only. The measured vertical earth pressures, lateral earth pressures, wall facing deflections, and global strains of geogrids from these three MSE wall sections were analyzed in this report. The following summary and conclusions can be made:

1. The calibration factors between global and local strains for primary and secondary geogrids used in the test wall sections ranged from 1.00 to 1.29.
2. The design of the test wall sections met the AASHTO requirements for internal and external stability. The capacity demanding ratios (CDRs) for the internal stability in the Class C (referred to the prediction type after the construction) design were much larger than those in the Class A (referred to the prediction type before the construction) design because the friction angle of the backfill soil used in the Class C design was higher than that in the Class A design. As a result, the lateral earth pressure was reduced.
3. The measured wall facing deflections increased with the wall height. The maximum deflections happened at the top of the wall. The maximum wall facing deflections in TS1 and TS2 were smaller than that in TS3, indicating that the inclusion of secondary geogrids reduced the wall facing deflections. The wall facing deflections at the top of the wall in three test sections (TS1, TS2, and TS3) during the construction were much less than those estimated by the empirical relationship of H/75 (H is the wall height).

4. The measured vertical earth pressures increased with the construction of the wall. The measured vertical stress close to the wall facing was higher than those away from the wall facing before the construction of the backslope because the lateral earth pressure from the retained soil resulted in potential overturning of the backfill soil and increased the bearing stress close to the wall facing. The measured vertical earth pressures close to the wall facing were lower than those away from the wall facing after the construction of the backslope because, as an eccentric load, the backslope led to overturning away from the toe of the wall.
5. In the test wall section without secondary geogrids, the measured lateral earth pressure increased approximately linearly with depth and was between the calculated active earth pressures and at-rest earth pressures using the actual friction angle of the aggregate. The measured earth pressures within the lower portion of the wall were close to the at-rest earth pressures because the existence of the embedment limited the wall deflection. However, the measured earth pressures within the upper portion of the wall were close to the active earth pressure because the wall deflection was sufficient to allow the backfill soil to be in an active state within the upper portion of the wall.
6. The measured lateral earth pressures in the test wall sections with secondary geogrids were approximately uniform with depth. The lateral earth pressures for the upper portion of the wall were close to the at-rest earth pressures because the existence of secondary reinforcement reduced the wall deflection.
7. The distribution of coefficient of lateral earth pressure was approximately uniform in the control section. However, the coefficients of lateral earth pressure decreased with depth in TS1 and TS2 when the depth was less than 20 ft. In addition, the coefficients of

lateral earth pressure in TS1 and TS2 were larger than that in TS3 because the inclusion of secondary reinforcement reduced the wall facing deflection.

8. The strains of the primary geogrids increased along the geogrids to reach a maximum value and then decreased to zero at a distance away from the wall facing. The distance of interaction between geogrid and backfill soil increased with the height of the wall. This result is consistent with that obtained by Leshchinsky et al. (2014).
9. The strains of the geogrids at the connections were very small and the corresponding connection forces were also very low. This result may be attributed to the fact that the strains due to the displacement of modular blocks during the compaction of the backfill soil before initial readings of geogrid strains were not taken. A similar finding of a low connection force was also noted by Leshchinsky et al. (2014).
10. The secondary reinforcements carried a portion of the tension force from the lateral earth pressures and reduced the tension force in the primary geogrids.

References

Abu-Hejleh, N., Zornberg, J.G., Wang, T., McMullen, M., & Outcalt, W. (2001). *Performance of geosynthetic-reinforced walls supporting the Founders/Meadows Bridge and approaching roadway structures. Report 2: Assessment of the performance and design of the front GRS walls and recommendations for future GRS abutments* (Report No. CDOT-DTD-R-2001-12). Denver, CO: Colorado Department of Transportation.

Allen, T.M., & Bathurst, R. (2013). Design and performance of 6.3-m-high, block-faced geogrid wall designed using K-Stiffness Method. *Journal of Geotechnical and Geoenvironmental Engineering, 140*(2), 1-12.

Allen, T.M., Christopher, B.R., & Holtz, R.D. (1992). *Performance of a 41-foot high geotextile wall* (Report No. WA-RD 257.1). Olympia, WA: Washington Department of Transportation.

American Association of State Highway and Transportation Officials (AASHTO). (2007). *AASHTO LRFD bridge design specifications* (4th ed.). Washington, DC: Author.

American Association of State Highway and Transportation Officials (AASHTO). (2012). *AASHTO LRFD bridge design specifications* (6th ed.). Washington, DC: Author.

ASTM C136-06. (2006). *Standard test method for sieve analysis of fine and coarse aggregates.* West Conshohocken, PA: ASTM International. doi: 10.1520/C0136-06, www.astm.org

ASTM D698-12e2 (2012) *Standard test methods for laboratory compaction characteristics of soil using standard effort (12 400 ft-lbf/ft3 (600 kN-m/m3)).* West Conshohocken, PA: ASTM International. doi: 10.1520/D0698-12E02, www.astm.org

ASTM D1196 / D1196M-12. (2012). *Standard test method for nonrepetitive static plate load tests of soils and flexible pavement components, for use in evaluation and design of airport and highway pavements*. West Conshohocken, PA: ASTM International. doi: 10.1520/D1196_D1196M-12, www.astm.org

ASTM D1556-07. (2007). *Standard test method for density and unit weight of soil in place by the sand-cone method*. West Conshohocken, PA: ASTM International. doi: 10.1520/D1556-07, www.astm.org

ASTM D2487-11. (2011). *Standard practice for classification of soils for engineering purposes (Unified Soil Classification System)*. West Conshohocken, PA: ASTM International. DOI: 10.1520/D2487-11, www.astm.org

ASTM D4318-10e1. (2010). *Standard test methods for liquid limit, plastic limit, and plasticity index of soils*. West Conshohocken, PA: ASTM International. doi: 10.1520/D4318, www.astm.org

ASTM D6637 / D6637M-15. (2015). *Standard test method for determining tensile properties of geogrids by the single or multi-rib tensile method*. West Conshohocken, PA: ASTM International. doi: 10.1520/D6637_D6637M-15, www.astm.org

ASTM D7181-11. (2011). *Method for consolidated drained triaxial compression test for soils*. West Conshohocken, PA: ASTM International. doi: 10.1520/D7181-11, www.astm.org

Bathurst, R.J., Allen, T.M., & Walters, D.L. (2002). Short-term strain and deformation behavior of geosynthetic wall at working stress conditions. *Geosynthetics International, 9*(5-6), 451-482.

Bathurst, R.J., Walters, D., Vlachopoulos, N., Burgess, P., & Allen, T.M. (2000). Full scale testing of geosynthetic reinforced walls. In J.G. Zornberg & B.R. Christopher (Eds.), *Advances in Transportation and Geoenvironmental Systems Using Geosynthetics* (pp. 201-217). Reston, VA: American Society of Civil Engineers.

Berg, R.R. (1993). *Guidelines for design, specification, and contracting of geosynthetic mechanically stabilized earth slopes on firm foundations* (Report No. FHWA-SA-93-025). Washington, DC: Federal Highway Administration.

Christopher, B.R., Gill, S.A., Giroud, J.P., Juran, I., Mitchell, J.K, Schlosser, F., & Dunnicliff, J. (1989). *Reinforced soil structures, Volume I. Design and construction guidelines and Volume II. Summary of research and systems information* (Report No. FHWA-RD-89-043). Washington, DC: Federal Highway Administration.

Desai, C.S., & El-Hoseiny, K.E. (2005). Prediction of field behavior of reinforced soil wall using advanced constitutive model. *Journal of Geotechnical and Geoenvironmental Engineering, 131*(6), 729-739.

Elias, V., & Christopher, B.R. (1997). *Mechanically stabilized earth walls and reinforced soil slopes, design and construction guidelines* (Report No. FHWA-SA-96-071). Washington, DC: Federal Highway Administration.

Google. (n.d.). Google Maps. Retrieved from http://maps.google.com

Han, J., & Leshchinsky, D. (2006). General analytical framework for design of flexible reinforced earth structures. *Journal of Geotechnical and Geoenvironmental Engineering, 132*(11), 1427-1435.

Koerner, R.M., & Koerner, G.R. (2011). The importance of drainage control for geosynthetic reinforced mechanically stabilized earth walls. *Journal of GeoEngineering, 6*(1), 3-13.

Leshchinsky, D. (2000). Alleviating connection load. *Geotechnical Fabrics Report, 18*(8), 34-39.

Leshchinsky, D., & Vulova, C. (2001). Numerical investigation of the effects of geosynthetic spacing on failure mechanisms of MSE block walls. *Geosynthetics International, 8*(4), 343-365.

Leshchinsky, D., Kang, B.J., Han, J., & Ling, H.I. (2014). Framework for limit state design of geosynthetic-reinforced walls and slopes. *Transportation Infrastructure Geotechnology, 1*(2), 129-164.

Ling, P., & Leshchinsky, D. (1996). *Mesa walls: Field data reduction, finite element analysis, and preliminary design recommendations*. Atlanta, GA: Tensar Earth Technologies, Inc.

Michalowski, R. (2000). Secondary reinforcement for slopes. *Journal of Geotechnical and Geoenvironmental Engineering, 126*(12), 1166-1173.

Perkins, S.W., Schulz, J.L., & Lapeyre, J.A. (1997). Local versus global strain measurement of a polymeric geogrid. *Journal of Testing and Evaluation, 25*(6), 576-583.

Pierson, M.C., Parsons, R.L., Han, J., & Brennan, J.J. (2011). Laterally loaded shaft group capacities and deflections behind an MSE wall. *Journal of Geotechnical and Geoenvironmental Engineering, 137*(10), 882-889.

Thielen, D.L., & Collin, J.G. (1993). Geogrid reinforcement for surficial stability of slopes. In *Geosynthetics '93 conference proceedings* (pp. 229-241). St. Paul, MN: Industrial Fabrics Association International.

Vulova, C., & Leshchinsky, D. (2003). *Effects of geosynthetic reinforcement spacing on the behavior of mechanically stabilized earth walls* (Report No. FHWA-RD-03-048). McLean, VA: Federal Highway Administration.

Yang, G., Ding, J.X., Zhou, Q.Y., & Zhang, B. (2010). Field behavior of a geogrid reinforced soil retaining wall with a wrap-around facing. *Geotechnical Testing Journal, 33*(1), 1-6.

Yang, G., Liu, H., Lv, P., & Zhang, B. (2012). Geogrid-reinforced lime-treated cohesive soil retaining wall: Case study and implications. *Geotextiles and Geomembranes, 35,* 112-118.

Yang, G., Liu, H., Zhou, Y., & Xiong, B. (2014). Post-construction performance of a two-tiered geogrid reinforced soil wall backfilled with soil-rock mixture. *Geotextiles and Geomembranes, 42*(2), 91-97.

Yang, G., Zhang, B., Lv, P., & Zhou, Q. (2009). Behaviour of geogrid reinforced soil retaining wall with concrete-rigid facing. *Geotextiles and Geomembranes, 27*(5), 350-356.

Yoo, C. (2004). Performance of a 6-year-old geosynthetic-reinforced segmental retaining wall. *Geotextiles and Geomembranes, 22*(5), 377-397.

Yoo, C., & Jung, H. (2004). Measured behavior of a geosynthetic-reinforced segmental retaining wall in a tiered configuration. *Geotextiles and Geomembranes, 22*(5), 359-376.

K-TRAN

KANSAS TRANSPORTATION RESEARCH AND NEW-DEVELOPMENT PROGRAM

AD ASTRA PER ASPERA

Kansas

Department of Transportation